

Determinants of Voltage-dependent Gating and Open-State Stability in the S5 Segment of *Shaker* Potassium Channels

Max Kanevsky and Richard W. Aldrich

From the Howard Hughes Medical Institute and Department of Molecular and Cellular Physiology, Stanford University School of Medicine, Stanford, California 94305

abstract The best-known *Shaker* allele of *Drosophila* with a novel gating phenotype, *Sh^F*, differs from the wild-type potassium channel by a point mutation in the fifth membrane-spanning segment (S5) (Gautam, M., and M.A. Tanouye. 1990. *Neuron*. 5:67–73; Lichtinghagen, R., M. Stocker, R. Wittka, G. Boheim, W. Stühmer, A. Ferrus, and O. Pongs. 1990. *EMBO [Eur. Mol. Biol. Organ.] J.* 9:4399–4407) and causes a decrease in the apparent voltage dependence of opening. A kinetic study of *Sh^F* revealed that changes in the deactivation rate could account for the altered gating behavior (Zagotta, W.N., and R.W. Aldrich. 1990. *J. Neurosci.* 10:1799–1810), but the presence of intact fast inactivation precluded observation of the closing kinetics and steady state activation. We studied the *Sh^F* mutation (F401I) in ShB channels in which fast N-type inactivation was removed, directly confirming this conclusion. Replacement of other phenylalanines in S5 did not result in substantial alterations in voltage-dependent gating. At position 401, valine and alanine substitutions, like F401I, produce currents with decreased apparent voltage dependence of the open probability and of the deactivation rates, as well as accelerated kinetics of opening and closing. A leucine residue is the exception among aliphatic mutants, with the F401L channels having a steep voltage dependence of opening and slow closing kinetics. The analysis of sigmoidal delay in channel opening, and of gating current kinetics, indicates that wild-type and F401L mutant channels possess a form of cooperativity in the gating mechanism that the F401A channels lack. The wild-type and F401L channels' entering the open state gives rise to slow decay of the OFF gating current. In F401A, rapid gating charge return persists after channels open, confirming that this mutation disrupts stabilization of the open state. We present a kinetic model that can account for these properties by postulating that the four subunits independently undergo two sequential voltage-sensitive transitions each, followed by a final concerted opening step. These channels differ primarily in the final concerted transition, which is biased in favor of the open state in F401L and the wild type, and in the opposite direction in F401A. These results are consistent with an activation scheme whereby bulky aromatic or aliphatic side chains at position 401 in S5 cooperatively stabilize the open state, possibly by interacting with residues in other helices.

key words: gating current • ion channel • site-directed mutagenesis • activation • cooperativity

introduction

Potassium channels exert a stabilizing influence over the membrane potential of excitable cells, shaping the patterns of their electrical activity and serving as targets for modulators and drugs. To perform this role, many potassium channels have evolved exquisite sensitivity to transmembrane voltage. The *Shaker* channel, a member of the family of voltage-gated (Kv)¹ potassium channels (Kamb et al., 1987; Papazian et al., 1987; Pongs et al.,

1988) has been studied extensively as a model system for mechanistic studies of K⁺ channel function.

Voltage-dependent gating refers to the conformational transitions that the channel protein can undergo in which intrinsic charged or dipolar groups (gating charges) move in response to changes in the membrane voltage. Structurally, voltage-gated potassium channels exist as tetramers of like alpha subunits (MacKinnon, 1991; Kavanaugh et al., 1992; Liman et al., 1992; Doyle et al., 1998), often in association with accessory subunits (Xu et al., 1998). Extensive site-directed mutagenesis of basic amino acids in the fourth transmembrane segment (S4) has confirmed their importance in the voltage-dependent gating of *Shaker* and other potassium channels (Liman et al., 1991; Papazian et al., 1991; Logothetis et al., 1992) and has shown that several S4 basic residues comprise a portion of the gating charge (Perozo et al., 1994; Aggarwal and MacKinnon, 1996; Seoh et al., 1996). In addition, in both *Shaker* and muscle sodium channels, the S4 has been shown to be translocated across the membrane in a

Portions of this work have been previously published in abstract form (Kanevsky, M., and R.W. Aldrich. 1994. *Biophys. J.* 66:A283; Kanevsky, M., and R.W. Aldrich. 1995. *Biophys. J.* 68:A136).

Address correspondence to Dr. R.W. Aldrich, Howard Hughes Medical Institute and Department of Molecular and Cellular Physiology, Beckman Center B-171, Stanford University School of Medicine, Stanford, CA 94305-5426. Fax: 650-725-4463; E-mail: raldrich@leland.stanford.edu

¹*Abbreviations used in this paper:* G(V), steady state voltage dependence of the open probability; Kv, voltage gated; Q(V), charge displacement versus voltage; S4, fourth transmembrane segment; S5, fifth membrane-spanning segment; wt, wild type.

voltage-dependent fashion correlating with the activation process (Yang and Horn, 1995; Larsson et al., 1996; Mannuzzu et al., 1996; Yang et al., 1996; Yusaf et al., 1996). Mutations of uncharged S4 and S4–S5 segment amino acids also exert strong effects on activation gating (Lopez et al., 1991; McCormack et al., 1991; Schoppa et al., 1992; Logothetis et al., 1993; Schoppa and Sigworth, 1998b), in particular influencing late cooperative transitions in the activation pathway (Smith-Maxwell et al., 1998b). There is evidence that an acidic residue in the S2 segment may be part of the gating charge and act as one of the countercharges for the S4 gating charges (Papazian et al., 1995; Seoh et al., 1996; Keynes and Elinder, 1999), but the nature of interactions between S4 residues with other regions of the channel remains unclear.

We have used a previously studied mutant *Shaker* allele as a starting point to help understand the role of the fifth membrane-spanning segment (S5) in activation gating and as a potential interacting partner for S4. *Sh^h* is the best known mutant *Shaker* allele that affects voltage-dependent gating in *Drosophila*. It differs from the wild-type sequence by a phenylalanine-to-isoleucine substitution located in the S5 transmembrane segment: F401I (Gautam and Tanouye, 1990; Lichtinghagen et al., 1990). Whereas most mutant *Shaker* alleles (e.g., *Sh^{KS133}*, *Sh^{I02}*) have a loss-of-function phenotype (Salkoff, 1983), eliminating the transient “A₁-type” potassium current and broadening the action potential (Tanouye et al., 1981; Salkoff, 1983; Tanouye and Ferrus, 1985; Wu and Haugland, 1985), *Sh^h* fly nerves fire rapid spikes that, because of failure to repolarize completely, occur in bursts (Tanouye et al., 1981; Tanouye and Ferrus, 1985). In *Sh^h* muscle fibers, A-type currents possess novel gating properties that have been reported as either shifting voltage dependence of activation and inactivation to a more positive range (Wu and Haugland, 1985) or speeding up the kinetics of inactivation and recovery (Salkoff, 1983). Close examination of the voltage dependence of steady state inactivation revealed that the slope is somewhat shallower in *Sh^h* than in the wild type (Wu and Haugland, 1985; Zagotta and Aldrich, 1990b), suggesting that this mutation may reduce the apparent activation gating valence. Kinetic modeling of *Sh^h* channels showed that changes in the rate and voltage dependence of deactivation could account for the altered gating behavior (Zagotta and Aldrich, 1990b). However, in the previous studies closing kinetics and steady state activation could not be directly measured in the native channels due to the presence of N-type inactivation.

Using the background of an NH₂ terminus-truncated version of the wild-type *Shaker* channel free of fast N-type inactivation (Hoshi et al., 1990), we introduced aliphatic point substitutions of the phenylalanine at po-

sition 401, the site of the *Sh^h* mutation. We asked whether changes in the size of the side chain at position 401 would lead to predictable consequences for voltage-dependent gating. The loss of apparent gating valence in *Sh^h* and other F401 substitutes is associated with a decrease in the voltage dependence of the backward transitions leading away from the open state. We extended the kinetic analysis of the wt and F401 mutants to determine which transitions between conformational states are disrupted by the substitutions. The physical picture of the channel as a tetramer of identical subunits (MacKinnon, 1991; Hurst et al., 1992; Liman et al., 1992; Doyle et al., 1998) restricts the interpretation of our results to schemes with fourfold symmetrical alterations in the gating parameters or with changes to concerted transitions between quaternary conformations of the channel.

Several gating mechanisms for potassium channels that incorporate independent and cooperative steps in the activation process have been proposed (Koren et al., 1990; Zagotta and Aldrich, 1990a; Tytgat and Hess, 1992; Bezanilla et al., 1994; McCormack et al., 1994; Zagotta et al., 1994b; Schoppa and Sigworth, 1998c). We use the aliphatic substitutions at F401 to test the ability of the type of models exemplified by Zagotta et al. (1994b) and Schoppa and Sigworth (1998c) to predict the mutants' divergent gating properties on the basis of physically interpretable alterations of just a few transitions. We conclude that F401 is involved in the cooperative stabilization of the open state.

materials and methods

Terminology

All mutant channel constructs were made in the ShBΔ6-46 background (Hoshi et al., 1990), a deletion mutant in which fast N-type inactivation has been disrupted. These parent channels will be referred to as wild type (wt), and channels containing further single amino acid substitutions will be designated AxxxB, where xxx is the position of the amino acid in the deduced sequence of ShB (Tempel et al., 1987). For gating current measurements, we used a version of the wild-type channel (free of N-type inactivation) containing the mutation W434F in the pore region that nearly completely abolishes ion conduction but not charge movement (Perozo et al., 1993; Yang et al., 1997). This construct will be referred to as wf, and point substitutions in its background will be termed wfAxxxB.

Site-directed Mutagenesis and Oocyte Expression

All conducting versions of constructs containing point substitutions in the S5 region were generated by synthetic oligonucleotide-directed cassette mutagenesis using the polymerase chain reaction. To record gating charge movement, a high-expression vector containing the W434F mutation (Perozo et al., 1993; Yang et al., 1997) was obtained from Ligia Toro (UCLA School of Medicine, Los Angeles, CA). We subcloned inserts containing the alanine and leucine substitutions for F401 into the W434F construct (wf). Fidelity of DNA synthesis was verified by dideoxy

termination sequencing (Sanger et al., 1977) of the region spanning the cassette insert. cRNAs were transcribed in vitro from plasmid templates, linearized with SacI or NdeI (HindIII for wf-based constructs), using the mMessage mMachine kit with T7 RNA polymerase (Ambion Inc.) and injected into *Xenopus laevis* oocytes 2–14 d before recording.

Electrophysiology

Patch-clamp recordings from oocytes were carried out using the Axopatch 200A amplifier (Axon Instruments) with borosilicate glass pipettes (initial tip resistances between 0.4 and 2 M Ω). Macroscopic ionic currents recorded in the inside-out and outside-out excised configurations (Hamill et al., 1981) were low-pass filtered at 5–10 kHz with an eight-pole Bessel filter (Frequency Devices, Inc.) and acquired online with sampling frequencies between 10 and 100 kHz using an ITC-16 interface board (Instrutek) and a Macintosh computer running Pulse software (HEKA Elektronik). In all experiments, care was taken to allow tail current kinetics to settle to a steady level for 3–5 min after patch excision to the inside-out configuration before acquiring data. Patches that showed significant drift in the tail current time constant over the course of the experiment were excluded from analysis. No series resistance compensation was used.

To improve the signal-to-noise ratio for gating current experiments, we used a high-performance cut-open oocyte clamp (CA-1; Dagan Inc.) (Tagliatalata et al., 1992; Stefani et al., 1994). Good voltage control and dynamic response were obtained by permeabilizing the lower dome with 0.3% saponin solution and using agar bridges filled with 1 M NaMES containing fine platinum-iridium wire. Low-resistance (<1 M Ω) glass microelectrodes were filled with 3 M KCl. Online series-resistance compensation was used. Linear leak and capacitive currents were subtracted using a P/–5 to P/–8 protocol from a holding voltage of –120 mV. Resulting traces were periodically compared with those obtained with a P/4 subtraction protocol from the holding voltage of +50 mV, and no consistent differences were noted. Records were low-pass filtered at 5–10 kHz.

A holding voltage of –100 mV was used except as noted in the text. All experiments were carried out at 20.0 \pm 0.2°C, unless otherwise indicated, using a feedback temperature controller device.

Solutions

For patch-clamp recordings, we used chloride-containing solutions. The external solution contained (mM): 140 NaCl, 5 MgCl₂, 2 KCl, 10 HEPES (NaOH), pH 7.1. The internal solution contained (mM): 140 KCl, 2 MgCl₂, 11 EGTA, 1 CaCl₂, 10 HEPES (*N*-methylglucamine), pH 7.2. To reduce the slowly activating native oocyte chloride conductances when using the cut-open clamp, we perfused nominally chloride-free solutions containing (top and guard chambers, mM): 110 NaOH, 2 KOH, 2 Mg(OH)₂, 5 HEPES (MES), pH 7.1; (bottom chamber, mM): 110 KOH, 2 Mg(OH)₂, 1 Ca(OH)₂, 10 EGTA, 5 HEPES (MES), pH 7.1.

Off-Line Analysis

Linear components of leak and capacitive currents were digitally subtracted. Macroscopic ionic and gating current records were analyzed further using Igor Pro (WaveMetrics) and custom-written software. Comparisons of the relative open probability versus voltage relationship among the wt and mutant channels were based on the isochronal (between 0.5 and 1 ms post-pulse) amplitude of their tail currents after variable test pulses because this approach does not rely on assumptions about the linearity of the open-channel *i*(V) or the reversal potential. This type of measurement is termed a steady state voltage dependence of the

open probability [*G*(V)] relation in this paper. We fit the *G*(V) data with Boltzmann functions raised to the fourth power (see Zagotta et al., 1994a), according to the equation,

$$P_0^{rel}(V) = [1/(1 + e^{-(V - V_{1/2})zF/RT})]^4,$$

where *z* is the apparent gating valence per channel subunit, *V*_{1/2} is the apparent mid-point of the voltage-dependent transition in each subunit, and *R*, *T*, and *F* have their usual thermodynamic meanings. The time course of current activation was fit with the exponential

$$I(t) = I_{max}(1 - e^{-(t - t_{delay})/\tau}),$$

beginning with the time of the half-maximal current amplitude. As a measure of delay in current turn-on, *t*_{delay} (the time-axis intercept of the fitted exponential function) was found to be widely variable between patches for the same channel species. Therefore, the independently measured time-to-half-maximum was used as an alternative indicator of the activation delay. Decaying exponential fits to the kinetics of tail currents were obtained using the equation

$$I(t) = I_{max}(e^{-(t - t_{delay})/\tau}),$$

Fits to experimental data and model simulations were performed using a Levenberg-Marquardt nonlinear least squares optimization algorithm.

Model simulations were done using BigChannel software, courtesy of Toshinori Hoshi and Dorothy Perkins (Howard Hughes Medical Institute, Stanford University, Stanford, CA). In brief, simulated macroscopic ionic and gating currents were calculated numerically using an Euler integration method, digitally filtered to match the corner frequency of an eight-pole Bessel filter used in obtaining the corresponding data, and subsequently analyzed in the manner identical to experimental traces. Model parameters were allowed to vary slightly in fitting individual families of records. The goodness of fit was ultimately assessed by eye. Model parameters used in each simulation are given in the figure legends.

results

The Sh⁵ Replica Mutation Alters Activation Gating of Shaker

A point mutation converting the first phenylalanine of the fifth transmembrane segment to isoleucine served as a replica of the *Sh⁵* mutation (Fig. 1 C). Families from patches expressing either wild-type or mutant F401I currents activate over a similar range of voltages and deactivate completely at the relatively depolarized tail potential of –65 mV (Fig. 1 A). Compared with the wt *G*(V) curve, F401I activation has a noticeably shallower voltage dependence (Fig. 1 B). The fourth power Boltzmann fits to the *G*(V) curves yield values of *z* of approximately four elementary charges (*e*₀) per wild-type subunit, which is similar to the estimated total charge displacement per channel of 12.5–14 *e*₀, obtained from direct gating current measurements (Schoppa et al., 1992; Aggarwal and MacKinnon, 1996; Noceti et al., 1996; Seoh et al., 1996). By contrast, the

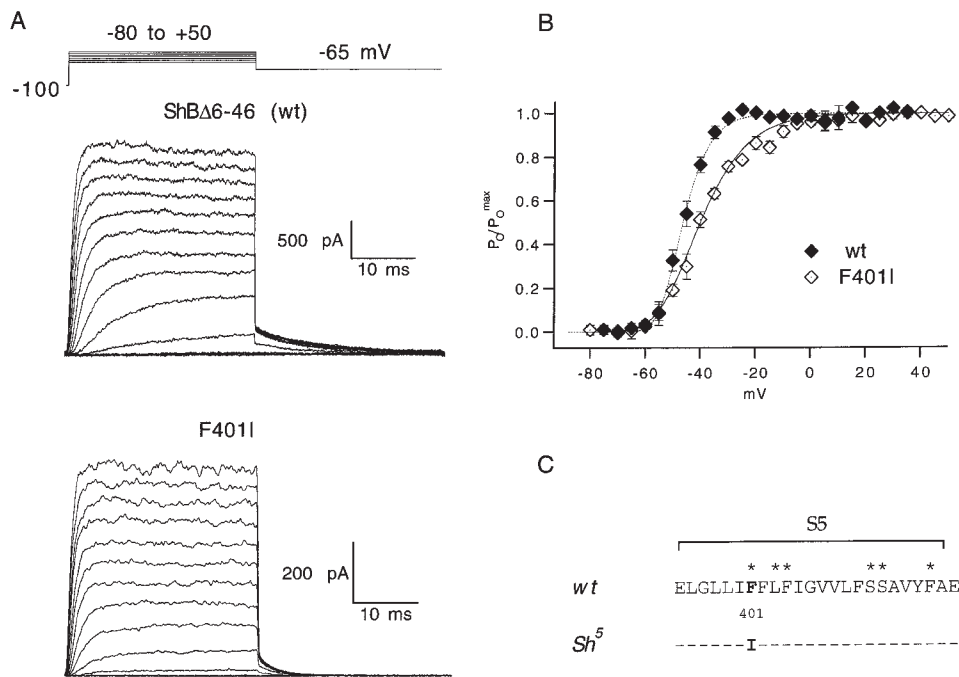


Figure 1. Steady state voltage dependence of the wild-type ShBΔ6-46 K channel and the F401I mutant. (A) Activation families were elicited from the holding potential of -100 mV with steps in 10 -mV increments between -80 to $+50$ mV, and tail currents were recorded at -65 mV, as indicated schematically above the traces. Patch-clamp records were obtained in the inside-out excised configuration (Hamill et al., 1981), digitized at 20 kHz, and low-pass filtered at 8 (wt) or 3 (F401I) kHz. (B) Relative conductance is plotted versus voltage. Conductances were normalized to the maximal value in each family and the results from different patches were averaged to obtain the means and standard errors shown (wt: $n = 5$; F401I: $n = 6$). Averaged $G(V)$ curves were fit with the fourth power of a Boltzmann function (see methods). The apparent

gating valence per subunit from these fits is reduced from $4.18 e_0$ for the wild type to $2.40 e_0$ for F401I. $V_{1/2}$ parameters from the fits are -56.3 mV for wt and -57.6 mV for F401I. (C) The amino acid sequence difference between wild-type *Shaker* and the neomorphic *Sh⁵* allele is localized to a single substitution in the S5 region: phenylalanine is mutated to isoleucine at position 401 (Gautam and Tanouye, 1990; Lichtinghagen et al., 1990). The sequence is shown using the standard single-letter amino acid code; dashes in the *Sh⁵* sequence indicate amino acid identity with wt. Asterisks mark the residues that were mutated in this study.

value of z for F401I is decreased to $2.4 e_0$, which implies that the mutation either reduces the amount of charge displacement in the channel, or alters the coupling between the charge-moving transitions and the channel opening.

If we consider a voltage-sensitive transition with associated charge displacement z in terms of transition-state theory, the voltage dependence of the forward and backward rates is determined by the charge movement before and after the transition state, respectively, and need not be equal. We asked if the diminished voltage dependence of the F401I mutant is associated primarily with forward or reverse transitions. A method to assess the forward rates in relative isolation from the backward transitions is illustrated in Fig. 2. The currents from wt and F401I channels activate with a sigmoidal delay, reflecting a multistep opening process. As the test potential is stepped to more positive values, channel opening kinetics accelerate for both the wt and F401I families. With sufficiently depolarizing voltage steps (i.e., more positive than -10 mV where the probability of opening for both channels nears saturation), the reverse rates can be considered negligible and the kinetics of activation are almost entirely determined by the forward rates. In this voltage range, the time course of activation has a complex multiexponential behavior but, for a class of models commonly used to describe

Shaker gating, the slowest exponential component has a time constant that is the inverse of the slowest forward rate (Zagotta et al., 1994a; Schoppa and Sigworth, 1998c). We find that a good single-exponential fit can be obtained to the latter phase of the trace beginning with the time at which currents reach their half-maximal amplitude (Fig. 2 A). The F401I mutant activates more rapidly and with less sigmoidal delay than the wild type. Time constants are voltage dependent, but the deduced amount of charge moved for these forward transitions is small and essentially unchanged between the wt and F401I channels (Fig. 2 B): 0.36 (see also Zagotta et al., 1994a) and $0.31 e_0$, respectively. F401I also produces a consistent decrease in the time-to-half-maximum current over the depolarized voltage ranges (Fig. 2, C and D).

Whereas the voltage dependence of the forward rates and, therefore, the amount of charge movement before the transition state, appears unaffected by the F401I mutation, the voltage dependence of the closing (deactivation) transitions, reflecting the charge movement "after" the transition state, is very sensitive to this change. The kinetics of deactivation were studied from currents recorded during channel closing (tail currents) at hyperpolarized potentials (negative to -60 mV) after maximally activating prepulses (Fig. 3, A and B). Deactivation follows a nearly single-exponential

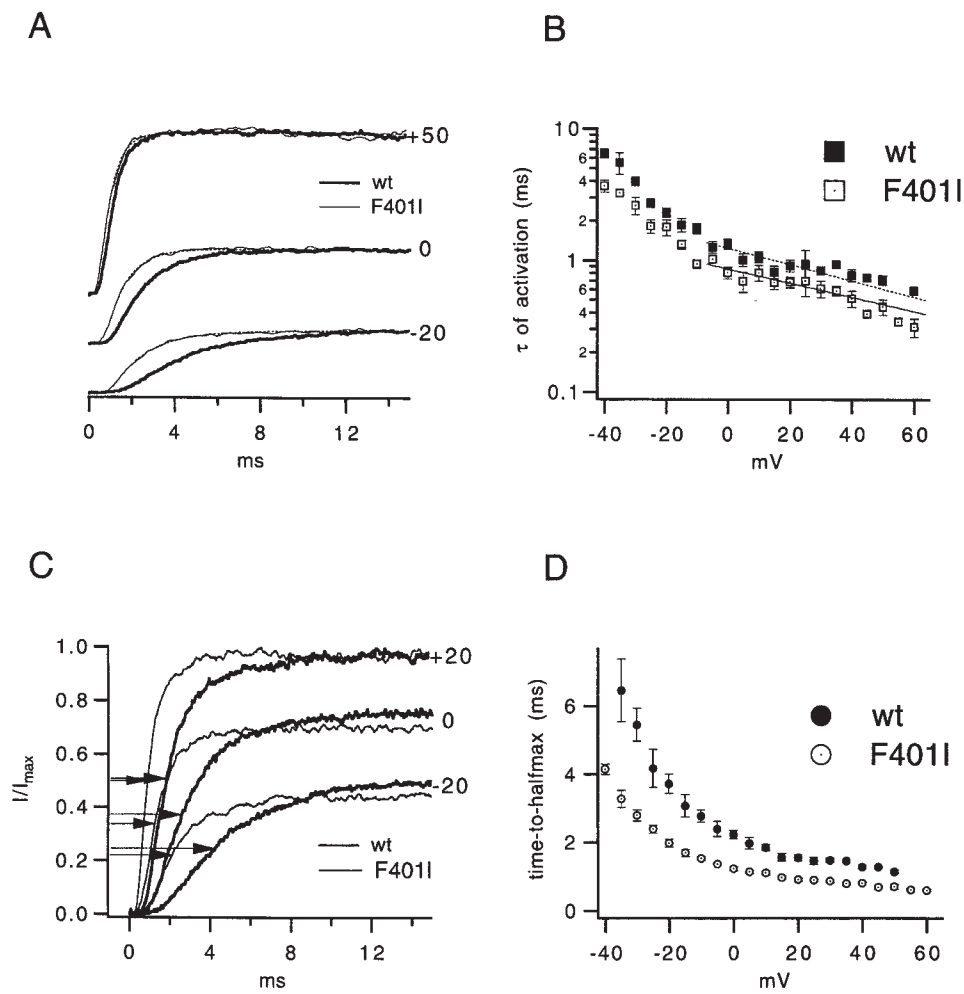


Figure 2. Kinetics and voltage dependence of forward transitions in the wild-type *Shaker* channel and the F401I mutant. (A) The time course of activation was compared in current traces obtained as in Fig. 1, with pulse voltages indicated on the right. Currents from wild-type and mutant channels were scaled to match maximal amplitudes at each of three voltage levels and fit with a single exponential function beginning at the time point corresponding to half-maximal current amplitude (see methods). Fits are superimposed on the traces as dotted curves. (B) Voltage dependence of the activation time constant. Values of the time constant, τ , derived from single-exponential fits from a number of patches (wt: $n = 7$; F401I: $n = 5$) were averaged and plotted against pulse voltage on semilogarithmic axes. Error bars represent the standard error of the mean. The time constant versus voltage relation was fit with a decaying exponential function above -10 mV, shown as solid (F401I) and dashed (wt) lines. The apparent charge associated with forward transitions late in activation, z_f , was calculated from the slope of the fitted line, and found to be $0.36 e_0$ for the wt and $0.31 e_0$ for F401I. (C) Difference in activation delay between wt

and mutant currents. Sets of representative traces recorded from two patches different from those in A are shown, with pulse voltage to the right of the traces. Current amplitudes for the $+20$ -mV traces in each family were set to unity. Arrows indicate the time points at which current amplitudes are half-maximal. (D) As a way to quantify the absolute activation delay, the mean time to reach half-maximum is displayed against pulse voltage for wt ($n = 8$) and F401I ($n = 5$) currents. The standard error of the mean is shown as error bars when it exceeds the size of a symbol.

time course in both channels, with the time constants from the fits displayed in Fig. 3 C against tail voltage. wt tail currents are not simply slower compared with F401I; the difference is greatest at -60 mV, but diminishes at very negative voltages and largely disappears below -160 mV (Fig. 3 C, inset). Kinetics of the tail currents in the wt are steeply potential dependent, with the apparent charge associated with the backward transitions, z_r , of $1.2 e_0$, consistent with a previous report (Zagotta et al., 1994a). This number may be an overestimate of the actual charge associated with the rate of any one individual backward transition because of the tendency of channels to reopen in a voltage-sensitive fashion at all but the most negative tail voltages (Schoppa and Sigworth, 1998a). In contrast to the wt, the apparent valence derived from voltage dependence of tail time constants in F401I is only $0.68 e_0$. Thus,

while the F401I mutant appears to move roughly the same amount of charge during the forward transitions late in the activation process, the mutation nearly halves the apparent charge movement associated with the early backward transitions. Therefore, the dominant effect on the kinetics of the F401I channels' return to the closed state is the speeding of the tail currents over all but the most negative voltages at which the determination of the tail time constant can become limited by the clamp response time. Our ability to observe deactivation in the absence of superimposed fast N-type inactivation allows us to study reverse transitions in relative isolation from other kinetic processes in the channel. Our results lend direct support to the earlier proposal by Zagotta and Aldrich (1990b) that the *Sh5* mutation affects the magnitude and voltage dependence of the reverse rate.

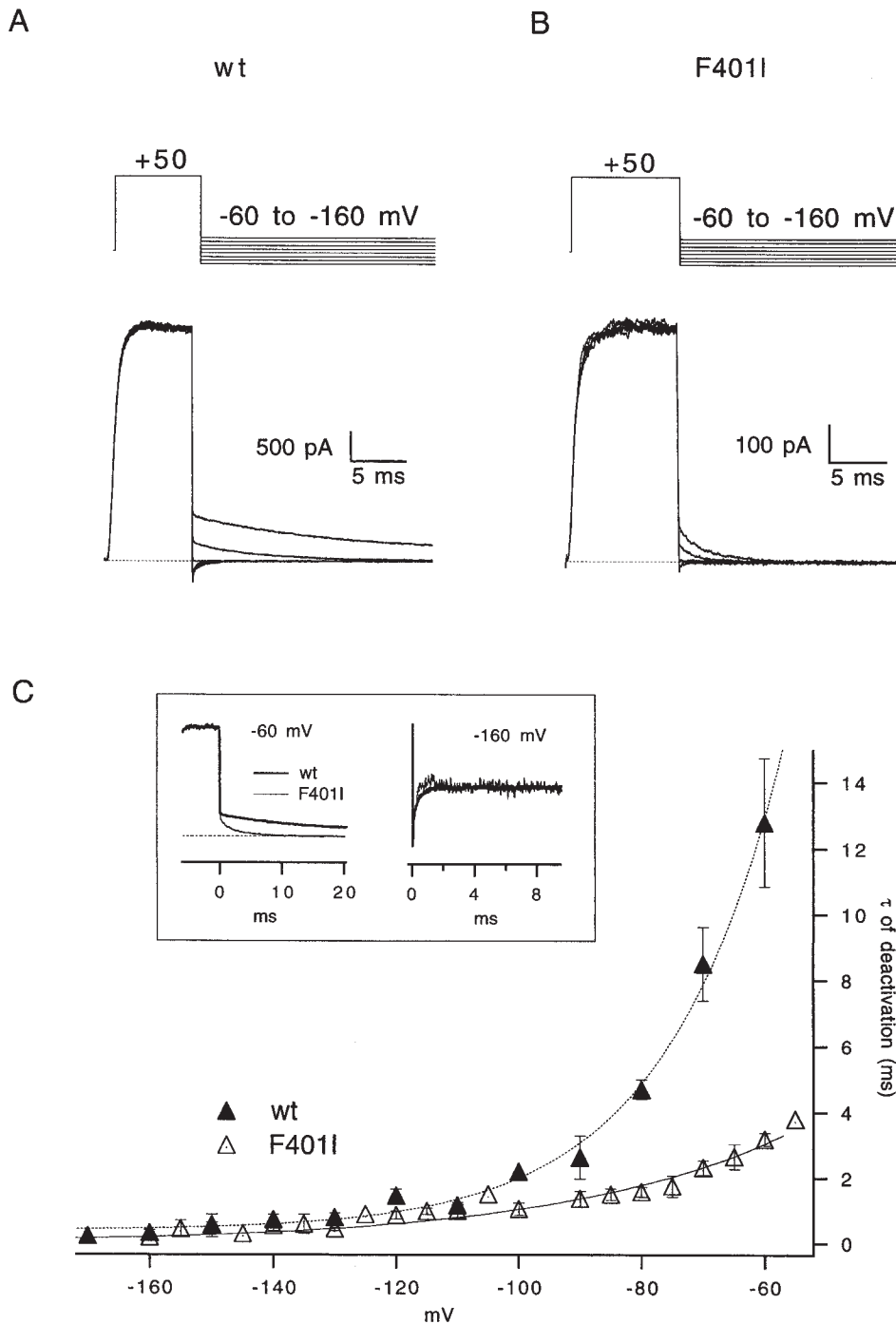


Figure 3. Alterations in the kinetics and voltage dependence of the closing transitions associated with the F401I mutation. (A and B) Deactivation families from wt (A) and F401I (B) patches were obtained with brief (8–10 ms) depolarizations to +50 mV, followed by steps to voltages between –60 and –160 mV in 10-mV increments, as indicated schematically above the traces. (C) Relaxations of the tail currents were fitted with a single exponential function (see methods). Means and standard errors of deactivation time constants, τ , from the fits are plotted against tail potential for patches containing wt ($n = 8$) and F401I ($n = 6$) channels. Average τ vs. voltage curves were computed and fitted with an exponential over the voltage range below –60 mV. Fits are shown as solid (F401I) and broken (wt) lines. The apparent charge associated with reverse transitions, z_r , was calculated from the steepness of the exponential voltage dependence of τ . z_r for the wt is $1.30 e_0$ whereas z_r for F401I is $0.68 e_0$. (Inset) Shown are superimposed wt and mutant tail currents recorded at –60 (left) and –160 (right) mV. The currents were scaled to match their peak amplitudes during the +50-mV prepulse. Note that the time scales are different so as to enable comparison of kinetic detail for the two species at both voltage extremes.

Comparison of S5 Phenylalanine Substitutions

F401 is one of five phenylalanines in the *Shaker* S5 sequence (at positions 401, 402, 404, 410, and 416; see Fig. 1 C). To investigate whether other amino acid substitutions in S5 have similar effects on activation gating, we conducted alanine mutagenesis of the four phenylalanines downstream (towards the carboxyl terminus) of F401 as well as other S5 hydrophobic residues (leucines at positions 396, 398, 399, 403, and 409, and serines at

positions 411 and 412), noting that it was an alanine substitution at F401 that resulted in the greatest effects (see below). Only F404A, F416A, L403A, S411A, and S412A gave rise to reliable ionic current expression. The results are shown in Fig. 4. The mutants' steady state activation voltage dependence shows few differences from the wt other than a small 1–10-mV depolarizing shift in most of the G(V) curves. The apparent valence of activation was not altered in any of the mu-

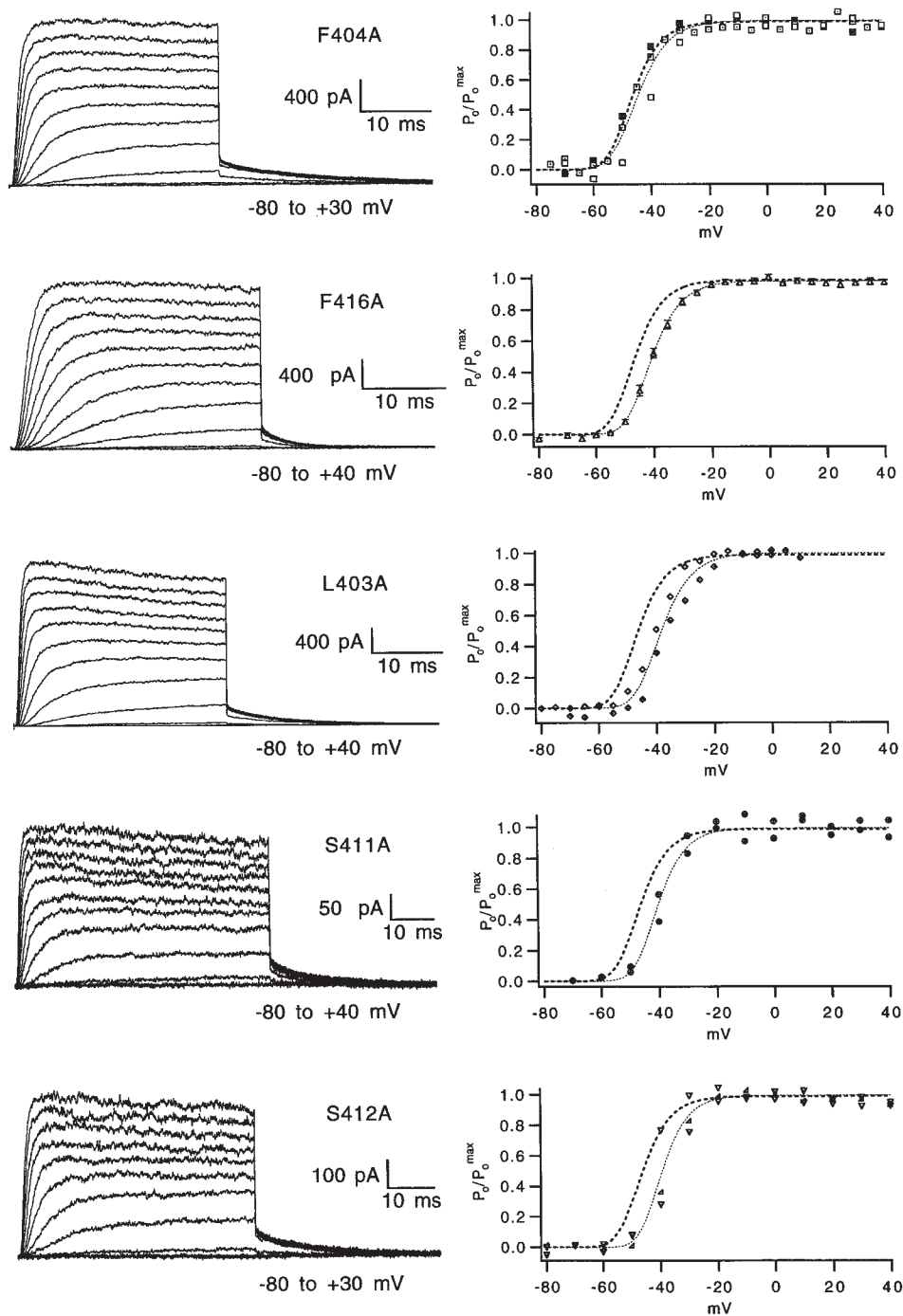


Figure 4. Alanine replacements in the S5 region and the steady state activation in *Shaker*. On the left are representative families recorded from inside-out patches containing the mutant channels indicated. Test steps were given in the voltage ranges shown under the traces in 10-mV increments. Tail voltage was -65 mV for all families. On the right, corresponding $G(V)$ relations are shown for each mutant; curves fitted to the wt $G(V)$ are included for comparison (shown as broken lines). For the F416A mutant, the mean of 12 experiments with its standard error is displayed. For the other mutants, combined data from three (F404A), two (L403A), two (S411A), and three (S412A) patches are shown. Thin lines through the data represent fits of the Boltzmann function raised to the fourth power (see methods), yielding the following estimates of apparent gating valence and midpoint of voltage-dependent transition: $z = 3.81 e_0$ and $V_{1/2} = -55.5$ mV (F404A); $z = 3.97 e_0$ and $V_{1/2} = -51.1$ mV (F416A); $z = 3.86 e_0$ and $V_{1/2} = -49.1$ mV (L403A); $z = 4.16 e_0$ and $V_{1/2} = -50.4$ mV (S411A); $z = 4.10 e_0$ and $V_{1/2} = -49.6$ mV (S412A).

tants. For L403A, these findings confirm earlier observations on channels with intact inactivation (Lopez et al., 1991; McCormack et al., 1991) that this residue, the fifth leucine in a putative heptad motif spanning the S4–S5 regions, plays at most a minor role in voltage-dependent gating. Results from the two serine substitutions imply that removal of the hydroxyl groups from the respective side chains does not alter the activation process.

Because the F404 residue is the least well conserved of S5 phenylalanines among the family of potassium channels, with alanine occurring at the equivalent site in, for example, Kv2.1, fShal and fShab, we were not surprised that the F404A substitution did not significantly alter activation or deactivation kinetics. In contrast, the position equivalent to F416 in *Shaker* channels only contains aromatic amino acids among voltage-gated potassium channels. We noted small but consis-

tent differences between the F416A mutant and the wild type. F416A currents have a more pronounced sigmoid delay in activation and more rapid deactivation kinetics. In summary, neither of the two downstream S5 phenylalanine-to-alanine mutations that produced functional channel expression, and none of the leucine and serine substitutions, influenced voltage-dependent gating to the degree evident for the F401 mutations.

Correlating Effects of F401 Mutations with Side Chain Properties

Because of the striking effects of the F401I substitution, we substituted other amino acids for the phenylalanine at 401 to investigate the role of side chain structure on

gating. We introduced individually three progressively smaller aliphatic amino acids leucine, valine, and alanine at that site. Fig. 5 A shows representative current families from these channels on different time scales to bring out the distinctive kinetic features of each channel type. In Fig. 5 B, the range of change induced by these mutations in the steady state voltage dependence of the relative open probability is shown. For comparison, previously described fits of a fourth power of the Boltzmann function to the wt and F401I data are also included. The F401V G(V) relationship is shallower than that of the wt, and similar in slope ($z_{app} = 2.5$) to the F401I mutant. However, the $V_{1/2}$ in F401V is positively shifted by ~ 5 mV compared with F401I. Steady state activation of the F401A mutant is the shallowest

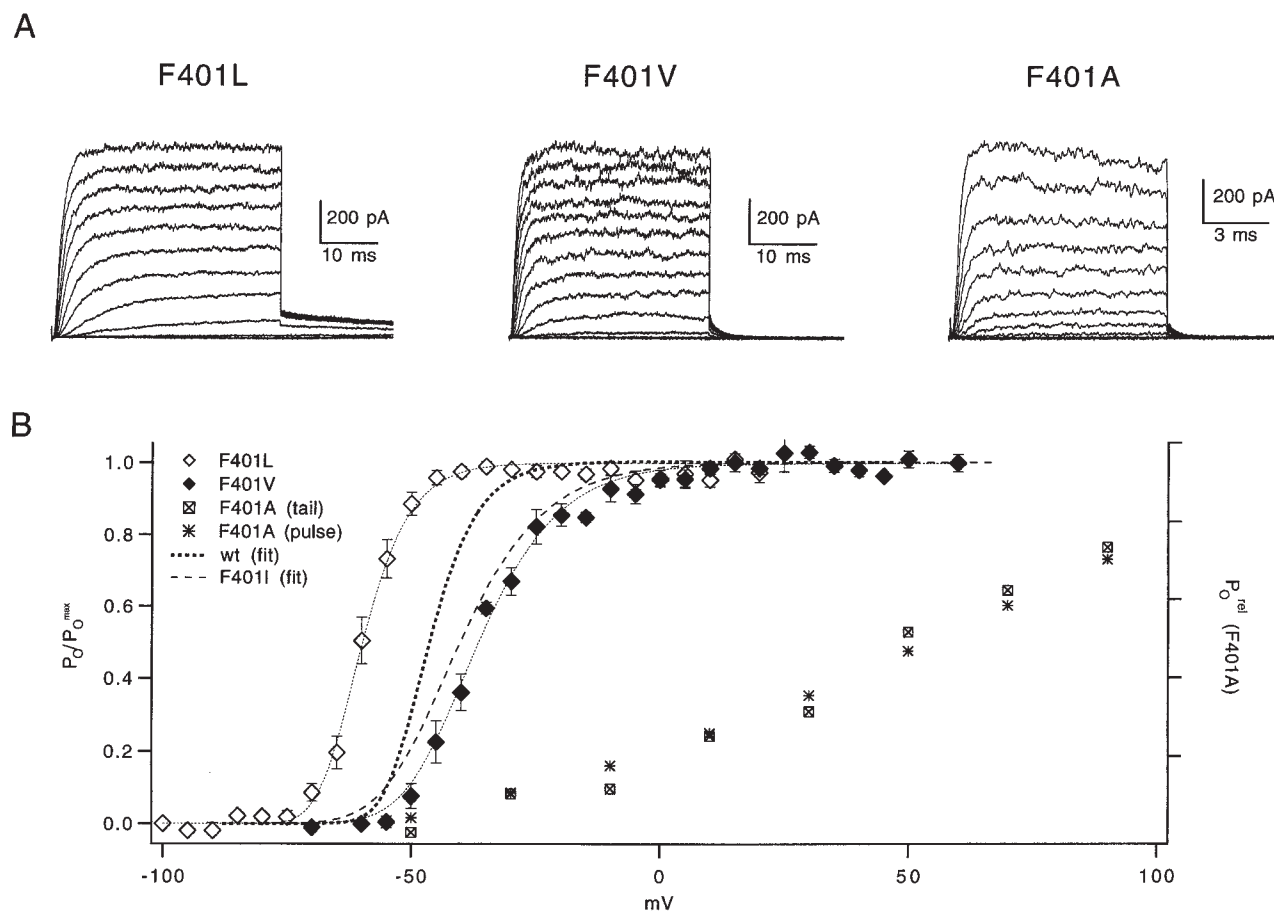


Figure 5. Aliphatic side-chain substitutions at position 401 affect the steady state voltage dependence of activation. (A) Families of macroscopic currents from patches expressing (left to right) F401L, F401V, and F401A channels were recorded as in Fig. 1. The voltage ranges for the three families were as follows (step increment in parentheses): -85 to $+25$ mV (10 mV) for F401L, -80 to $+60$ mV (10 mV) for F401V, and -80 to $+160$ mV (20 mV) for F401A. Note the faster time scale for the F401A family used to resolve its kinetic features. (B) Relative conductance versus voltage relationships for the three mutants are shown. For comparison, fits to G(V) curves for the wt and F401I channels are reproduced from Fig. 1. F401L and F401V data are plotted as means \pm SEM of eight and nine families, respectively. Averaged G(V) data were fitted with the fourth power of a Boltzmann function, as previously described, giving apparent z of 4.25 and 2.52 e_0 , and $V_{1/2}$ of -69.7 and -53.1 mV for F401L and F401V, respectively. For the F401A experiment shown (representative of 11 patches), G(V) was measured either as the chord conductance assuming the reversal potential of -80 mV (denoted "pulse"), or as the isochronal tail current amplitude (denoted "tail"). The characteristic failure of the steady state conductance to reach a maximum within the attainable voltage range prevented meaningful normalization of the F401A G(V).

($z_{app} < 0.5 e_0$); in fact, the G(V) relationship fails to reach saturation at voltages in excess of +150 mV in five patches, and is therefore displayed on a dimensionless y axis. Unexpectedly, introduction at position 401 of a leucine, an amino acid chemically most similar to the isoleucine, carried nearly opposite consequences compared with the *Sh⁵* replica mutation F401I. The F401L mutant has a G(V) relation as steep as that of the wt ($z_{app} = 4.25$) but with the midpoint of the activating transition shifted negatively ($V_{1/2} = -69.7$ mV), the only mutant in this study to do so.

A look at the activation time course on the expanded time scale in Fig. 6 A underscores that all channels bearing aliphatic substitutions for phenylalanine at position 401 activate more rapidly than the wt for a given voltage. Whereas F401L channels are least different from the wt, 401 isoleucine and valine channels are similar to each other and have faster kinetics than leucine channels; alanine channels are the fastest by far over all voltages. Quantitatively, Figs. 2 B and 6 B show that the voltage dependence of activation time constants measured late in the activation process is similarly weak no matter which of the five residues is at position 401, with the apparent valence associated with the forward transitions, z_f , ranging from 0.32 to 0.42 e_0 . The absolute values of the time constants, τ , are comparable except for F401A, in which they are significantly diminished. Regardless of whether F401 mutations diminish steady state voltage dependence of the currents, the voltage dependence of the forward rate, z_f , remains in the wt range.

We expected that, as in the case of *Sh⁵* (F401I), the other aliphatic substitutions would preferentially perturb deactivating transitions. In Fig. 7 A, time constants from fits to tail current relaxations are plotted for the leucine, valine, and alanine mutations. For comparison, fits to the voltage dependence of the deactivation time constant, τ , from wt and F401I are also included. The tail time constants of F401L currents are slower than those of the wt but have similarly steep voltage dependence. Deactivation kinetics of F401V ($z_f = 0.74 e_0$) are nearly the same as those of F401I, and F401A deactivation appears to be nearly voltage independent to the best of our ability to analyze its very rapid kinetics. This finding provides a ready explanation for the very shallow G(V) of F401A. In wild-type *Shaker*, a greater proportion of the total gating charge movement occurs after the transition state (Zagotta et al., 1994a), and its loss will be reflected in the diminished voltage dependence of the steady state gating parameters. On the other hand, the notable decrease in the backward rates and modest increase in the forward rates seen in F401L imply that some of the gating equilibria for this channel are biased toward the open state compared with the wt, which is consistent with the finding of a negatively

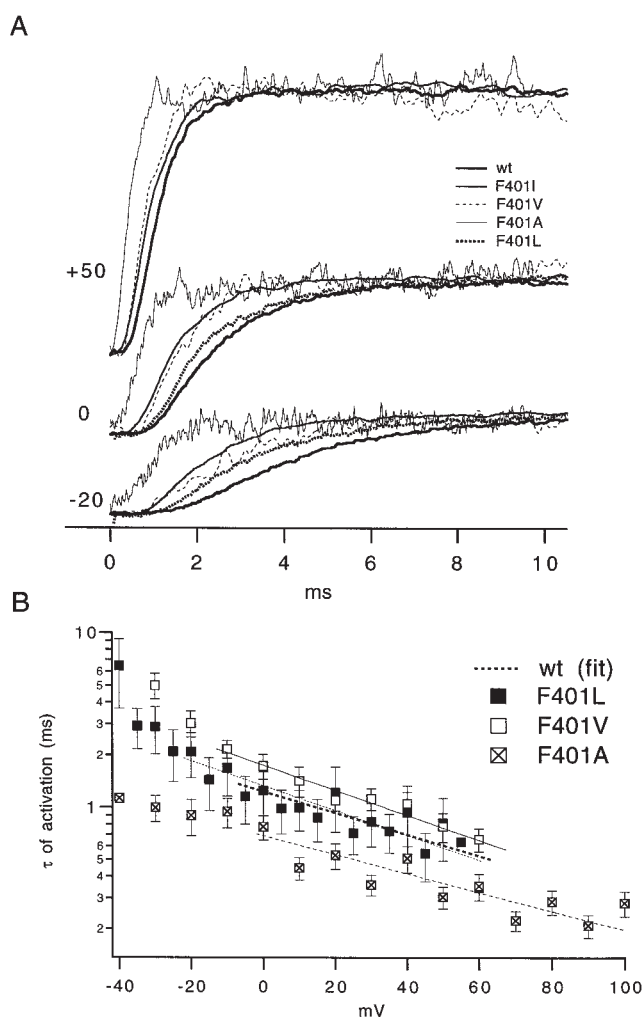


Figure 6. Effects of replacing phenylalanine 401 with aliphatic residues on the activation kinetics and voltage dependence. (A) Representative current traces from wt, F401I, F401V, F401A, and F401L patches were superimposed and scaled to match at their peaks. Pulse voltages are indicated on the left. (B) A semilogarithmic plot of the activation time constants (mean \pm SEM), determined from fitting an exponential function to the activation time course (see methods), is shown for the F401L ($n = 12$), F401V ($n = 12$), and F401A ($n = 11$) mutants. From the steepness of the exponential fit to the τ versus voltage relation, apparent valence associated with the forward transitions, z_f , was found to be 0.41 e_0 for F401L, 0.42 e_0 for F401V, and 0.32 e_0 for F401A. Fits are shown as thin solid and broken lines; for comparison, a fit to the wt activation τ is reproduced from Fig. 2 as a thick broken line.

shifted G(V) relation. Fig. 7 B depicts families of current traces from the two mutants that differ the most in their tail kinetics. Currents from the F401L and F401A families are shown on the same time scale to illustrate that there is more than an order of magnitude difference in the tendency of these channels, once activated, to remain in (or near to) the open state long after the end of a depolarizing voltage pulse. Note that even at

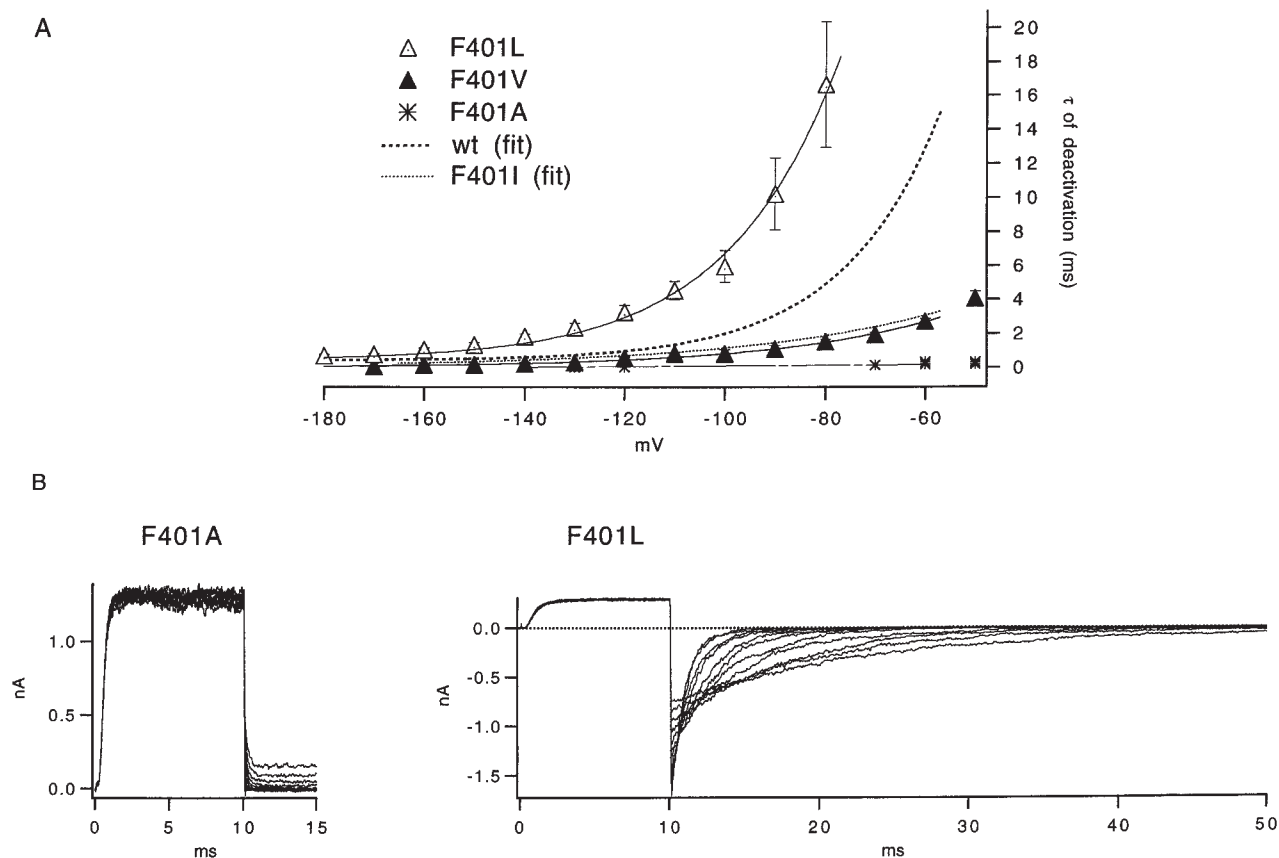


Figure 7. Substitutions at position 401 affect deactivation. (A) Deactivation time constants for the F401L, F401V, and F401A mutant channels were obtained from single exponential fits to currents during channel closing. The time constants, τ , are plotted as a function of tail potential and fitted with an exponential. For F401L and F401V, results are shown as the mean \pm SEM of 8 and 10 experiments, respectively. Due to the bandwidth limitations on our ability to fully resolve closing kinetics in the F401A mutant, results from the two best patches are shown at selected voltages. For comparison, fits to wild-type and F401I deactivation curves from Fig. 3 are also included. The voltage dependence of deactivation τ yielded apparent z values of $1.15 e_0$ for F401L, $0.74 e_0$ for F401V, and $<0.5 e_0$ for F401A. (B) Differences of deactivation kinetics are illustrated with the tail families of the F401A and F401L mutants, shown on the same time scale. The F401A family (left) was recorded under standard ionic conditions (see methods) from an inside-out patch, sampled at 100 kHz and low-pass filtered at 9.5 kHz. Tail voltage ranged between -20 and -170 mV in 10-mV increments. The F401L currents (right) were recorded from an outside-out patch with symmetrical 140 mM K^+ as the permeant cation. Increasing external K^+ from 2 to 140 mM does not significantly affect tail kinetics of this channel (data not shown, but see Zagotta et al. (1994a)). Tail voltage was stepped to between -80 and -180 mV in 10-mV increments. For both families, a 10-ms pulse to $+50$ mV preceded the steps to the tail potentials.

fairly depolarized tail potentials F401A channels relax to a new steady state level on a very rapid time scale.

Because several F401 mutants accelerate deactivation of macroscopic ionic currents, we hypothesized the faster rates for leaving the open state by deactivation should decrease the mean time spent in the open state. F401I has a unitary conductance similar to the wt but briefer open times (mean 2 vs. 4 ms in the wt), consistent with its faster deactivation kinetics. Single F401A channels show extremely brief, incompletely resolved openings that are seen promptly at the start of the test pulse (data not shown). Bandwidth limitations of the recording equipment did not allow us to pursue quantitative analysis of these channels, but qualitatively their behavior supports the hypothesis that isoleucine and

especially alanine mutants accelerate transitions from the open state that reverse the activation sequence.

Gating Charge Movement in the F401 Mutants

One possible explanation for the reduction in the apparent valence of channel opening in *Sb*⁵ and related F401 mutants is an alteration in the coupling among charge-moving transitions. This could take the form of a transition (or transitions) that the channel must undergo during opening that has a voltage midpoint shifted far in the positive direction relative to the wt, such as has been proposed for several S4 and S4-S5 linker mutations (Schoppa et al., 1992; Perozo et al., 1994; Schoppa and Sigworth, 1998b; Smith-Maxwell et

al., 1998a,b). Gating charge measurements from such a mutant will reveal a separation of charge components along the voltage axis, giving rise to an inflection or a frank shoulder in the total steady state charge displacement versus voltage [Q(V)] relationship (Ledwell and Aldrich, 1999). Therefore, we studied Q(V) relationships for the wt and two mutants with very different apparent gating valences.

Families of gating currents from the wf and the wfF401L and wfF401A mutants are shown in Fig. 8. The gating currents are shown superimposed and staggered to facilitate comparison of the development of kinetic features with changes in voltage. The wf ON gating cur-

rents (I_g^{ON}) have a rising phase, appear at negative voltages, and show a slow decaying component in the voltage range where channels open. This latter component accelerates with further depolarizations. The overall time course of the I_g^{ON} decay becomes faster in the order wf, wfF401L, and wfF401A, consistent with the faster time course of ionic current activation observed in the corresponding conducting species, although the F401A gating currents are accelerated to a lesser extent than the corresponding ionic currents. A prominent rising phase and slow decay appear in the wf OFF currents (I_g^{OFF}) at the voltages where there is a slow phase of the I_g^{ON} decay, consistent with published observa-

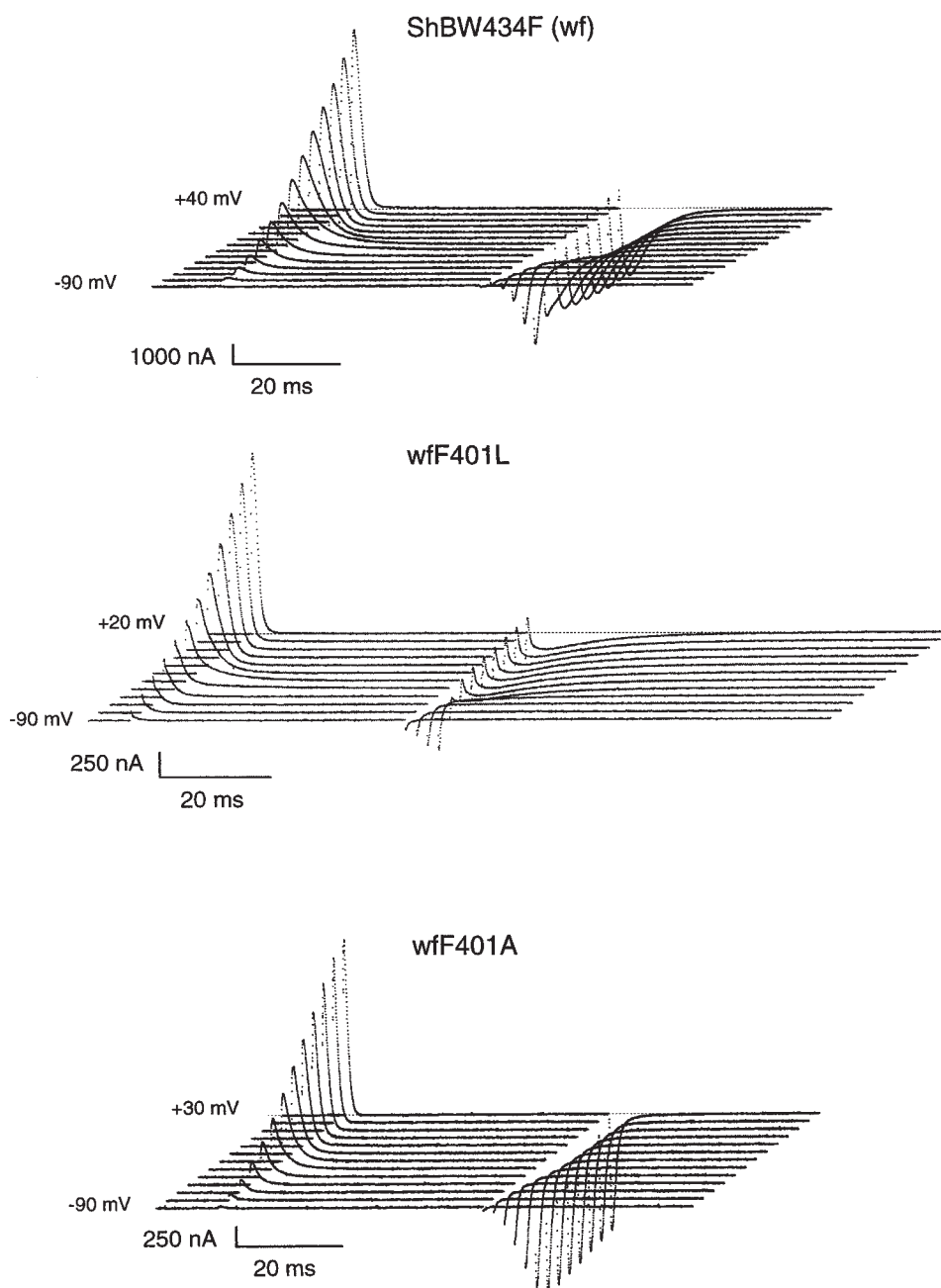


Figure 8. Gating charge movement in the wild type and channels containing F401L and F401A mutations. Gating currents were recorded from non-conducting channels containing the indicated mutations using a cut-open oocyte voltage clamp, digitized at 20 kHz (42 kHz for wfF401A) and low-pass filtered at 10 kHz. Traces elicited by steps to the voltages indicated on the left, beginning from and returning to the holding potential of -100 mV, are shown staggered to facilitate the kinetic comparison. Chloride-free standard solutions were used (see methods).

tions from the cut-open oocyte clamp. (Perozo et al., 1992; Bezanilla et al., 1994; Stefani et al., 1994). The most notable change introduced by the wF401L mutation is the profound slowing of the OFF gating charge return at voltages where the channel opens. In contrast, wF401A all but abolishes the slowing of I_g^{OFF} . The correlation between faster OFF gating charge return and faster deactivation of ionic currents is more consistent with the slowing of OFF charge due to a stabilization of the open state rather than to channels entering a C-type inactivated state (see Chen et al., 1997).

Steady state $Q(V)$ relationships for the three channels were computed from the integral of the I_g^{OFF} after a test pulse. The integral of the I_g^{ON} , while not shown, agreed closely. Fig. 9 A shows that the wf $Q(V)$ curve has a characteristically shallow base and steeper upper portion (see also Stefani et al., 1994). The wF401L $Q(V)$ relation is negatively shifted relative to the wf, similar to the relationship between the $G(V)$ of F401L and the wt. For this mutant, channel opening seems to follow closely the displacement of the voltage-sensing charges. wF401A has detectable charge movement at more negative voltages than the wf, but its $Q(V)$ slope is somewhat shallower. However, we did not detect any obvious inflections reflecting the movement of an additional component of the gating charge in the wF401A $Q(V)$ curve at voltages above 0 mV and extending even beyond +100 mV. Therefore, we conclude that the reduction in the apparent voltage dependence of activation is not the result of altered coupling of activation pathway transitions carrying significant amounts of charge movement. It is likely that this mutation affects an activating transition that moves only a small amount of charge and thus would not perturb the overall shape of the $Q(V)$ curve.

We can compare the kinetics of the ON gating currents by fitting their decay phase with an exponential time constant. I_g^{ON} is not well described by a single exponential at all voltages but, above -20 mV, these fits are useful as a way of assessing the overall kinetics of forward transitions in the channel. When these time constants are plotted against voltage for the wf and the wF401L and wF401A mutants (Fig. 9 B), the rates of forward transitions are the fastest for wF401A, followed by wF401L and the wf channel. This mirrors the relationship among the activation time constants of ionic currents from the corresponding conducting channels. The voltage dependence for the movement of the charge "before" the transition states (z_f) is conserved for the three channels, ranging between 0.57 and 0.63 e_0 . These values are similar to those estimated from ionic current measurements (Fig. 6) and place important constraints on kinetic modeling of the early steps in channel activation.

The changes in both the ionic and gating currents re-

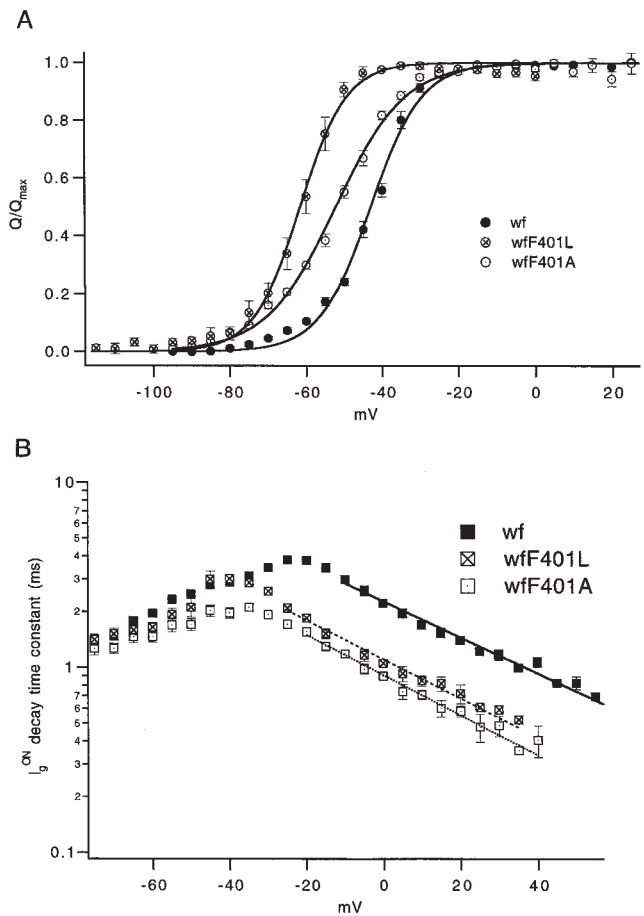


Figure 9. F401 substitutions affect the steady state charge transfer and kinetics of the forward transitions. (A) Relative charge versus voltage relations were computed for the wf, wF401L, and wF401A channels by integrating the gating current during the -100-mV post-pulse (I_g^{OFF}). Normalized $Q(V)$ relations from a number of experiments were averaged and plotted as a function of test voltage as mean \pm SEM (wf: $n = 17$; wF401L: $n = 10$; wF401A: $n = 12$). The fitted lines through the data are the Boltzmann function predictions for channels with independent and identical subunit transitions with the following values of voltage midpoint ($V_{1/2}$) and associated charge displacement (z): -43 mV and 3.73 e_0 , -61.6 mV and 4.14 e_0 , and -52.3 mV and 2.76 e_0 , for wf, wF401L, and wF401A, respectively. (B) The decay phase of the I_g^{ON} was fitted with a single exponential and the time constants are plotted against pulse voltage for the wf ($n = 11$), wF401L ($n = 8$), and wF401A ($n = 8$) channels. From the exponential fits of the voltage dependence, beginning at -10, -25, and -20 mV, the estimate z_f of the charge associated with the forward transitions is 0.57, 0.61, and 0.63 e_0 , for wf, wF401L, and wF401A, respectively.

veal alterations in the voltage dependence and magnitude of the reverse rates out of the open state with the F401 residue replacements. The time course and voltage dependence of the forward activation rates are much less affected. These results suggest that the F401 mutations alter the energetic stability of the open state relative to closed states. Alterations in gating by

changes of noncharged residues in the S4 segment have been interpreted in terms of a change in the energetics of a final cooperative opening step (Smith-Maxwell et al., 1998b; Ledwell and Aldrich, 1999). An alteration in the cooperative stabilization of the open state could likewise lead to the observed behavior of the F401 mutations. In the following section, we test this hypothesis more directly using previously developed experimental protocols to elucidate the cooperative interactions between channel subunits (Zagotta et al., 1994a; Smith-Maxwell et al., 1998b; Ledwell and Aldrich, 1999).

Behavior of Ionic Currents Indicates Nonindependence of Subunits

Shaker ionic currents activate upon depolarization with a delay, giving rise to a sigmoidal time course. This sigmoidicity arises from the multi-step nature of the activation process. Voltage dependence in the sigmoidicity of ionic currents is a diagnostic feature of deviation

from subunit independence in activation (Zagotta et al., 1994a; Smith-Maxwell et al., 1998a,b). Sigmoidicity is preserved in the mutant channels F401L and F401A (Fig. 10 A), although their overall kinetics and the absolute amount of delay vary. For a noncooperative model of channel activation that postulates n independent first-order voltage-dependent processes (Hodgkin and Huxley, 1952; Cole and Moore, 1960), it can be shown that sigmoidicity will be the same for a given n at all test voltages, and the time- and amplitude-scaled traces will superimpose. Over the voltage ranges shown, wt and F401L channels clearly display deviations from the independent scheme. Sigmoidicity is greater at higher than at lower voltages, but appears to reach a saturating value when the voltage is in the range of maximal steady state activation (reached near or below 0 mV for both of these channels). Zagotta et al. (1994a) used this observation in wt *Shaker* to argue for a form of cooperativity that acts to slow the first closing transition from the open state causing the current waveform at lower voltages to be close to a monoexponential func-

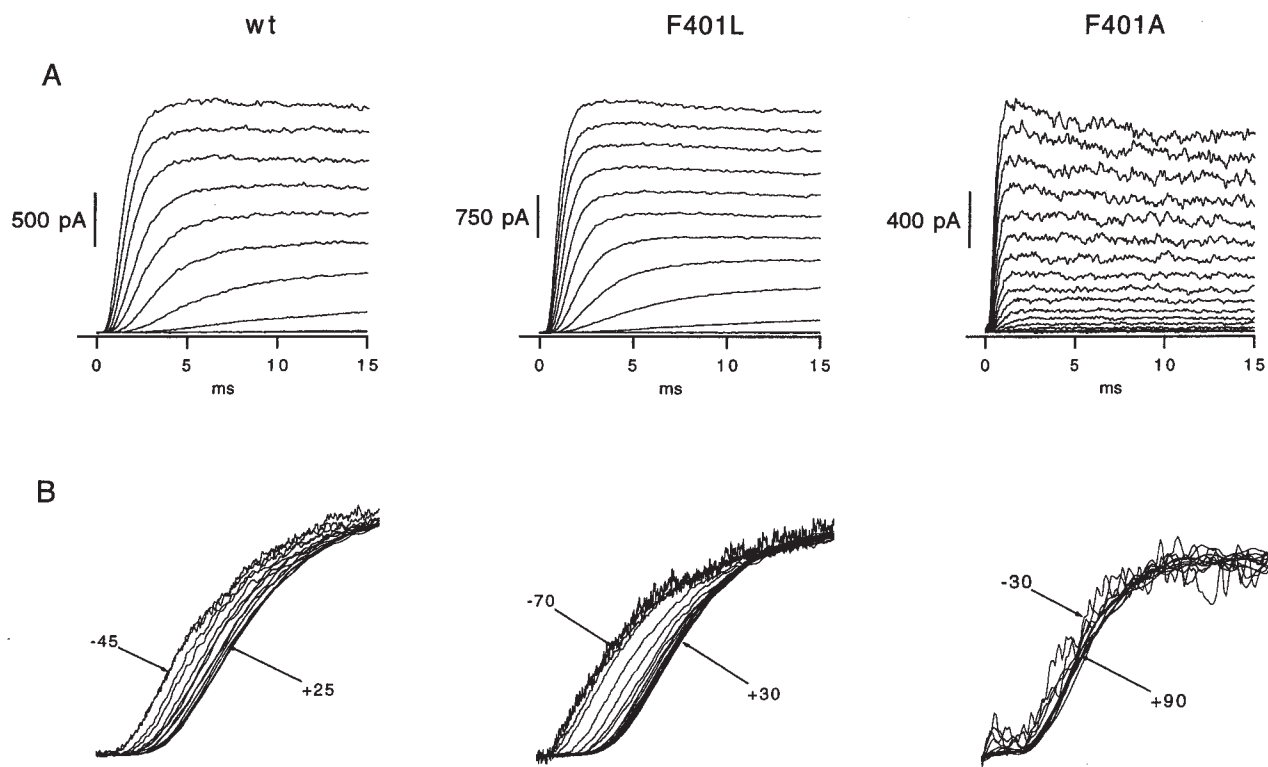


Figure 10. Mutations of F401 and cooperative gating: sigmoidicity. (A) Activation families of wt currents taken at voltages between -65 and 25 mV, F401L (-80 to $+30$ mV), and F401A (-70 mV to $+90$ mV) in 10 -mV increments. (B) Data transformed to normalize the current amplitude and overall speed of activation for the voltages shown. Sigmoidicity is defined as the amount of initial delay relative to the overall rate of activation. Its voltage dependence can be visualized by following transformation (Zagotta et al., 1994a). The currents from different voltage steps are first scaled to match at their peaks. Then the time derivative of the current waveform is determined at the time when current amplitude is half maximal. In general, it is at that point that the slope is the steepest. All the records in the family are then expanded or compressed along the time axis so that their derivatives at half-maximum match. This transformation results in parallel curves whose relative displacement along the x axis is the measure of sigmoidicity. The noisier traces correspond to lower voltages. Data were filtered at between 8 and 10 kHz and sampled every 20 – 50 μ s.

tion because it is limited by the slow final step (see also Smith-Maxwell et al., 1998a,b; Ledwell and Aldrich, 1999). From the F401L records, it is apparent that the smaller amount of sigmoidicity at the lower voltages is at least as pronounced as in the wt (note that the steady state activation in F401L is shifted negatively relative to the wt by 15–20 mV). On the other hand, over the voltage range between –40 and +90 mV, channels with an alanine substitution at F401 do not display the clear increase in the amount of sigmoidicity with higher depolarizations seen with the wt and F401L. The F401A mutant acts as though there is no rate-limiting transition present at the lower voltages, implying that the leaving rate from the open state is not slowed relative to the predictions of a mechanism with independently gating subunits.

We sought to confirm further that the mutations at F401 alter the deviation from independence seen in wt channels upon entering the open state. As originally de-

scribed by Cole and Moore (1960), multistep activation gating results in greater delay in current turn-on when the channels are subjected to progressively more negative voltages before the test pulse. The greater delay occurs as the equilibrium distribution of channels among closed states shifts in favor of the states most distant from the open state. For an independent gating scheme, a family of current waveforms corresponding to different prepulse voltages becomes superimposable simply by a translation along the time axis that allows for the amount of delay lost or gained. These transformations of wt, F401L, and F401A currents are shown in Fig. 11. In wt, over the voltage range between –140 and –70 mV, there is almost no current activation during the prepulse, and the corresponding traces at 0 mV are parallel and superimposable by a shift along the time axis. However, at the prepulse voltages of –50 and –40 mV, wt channels open with nonnegligible probability and the 0-mV current waveforms cannot be superimposed

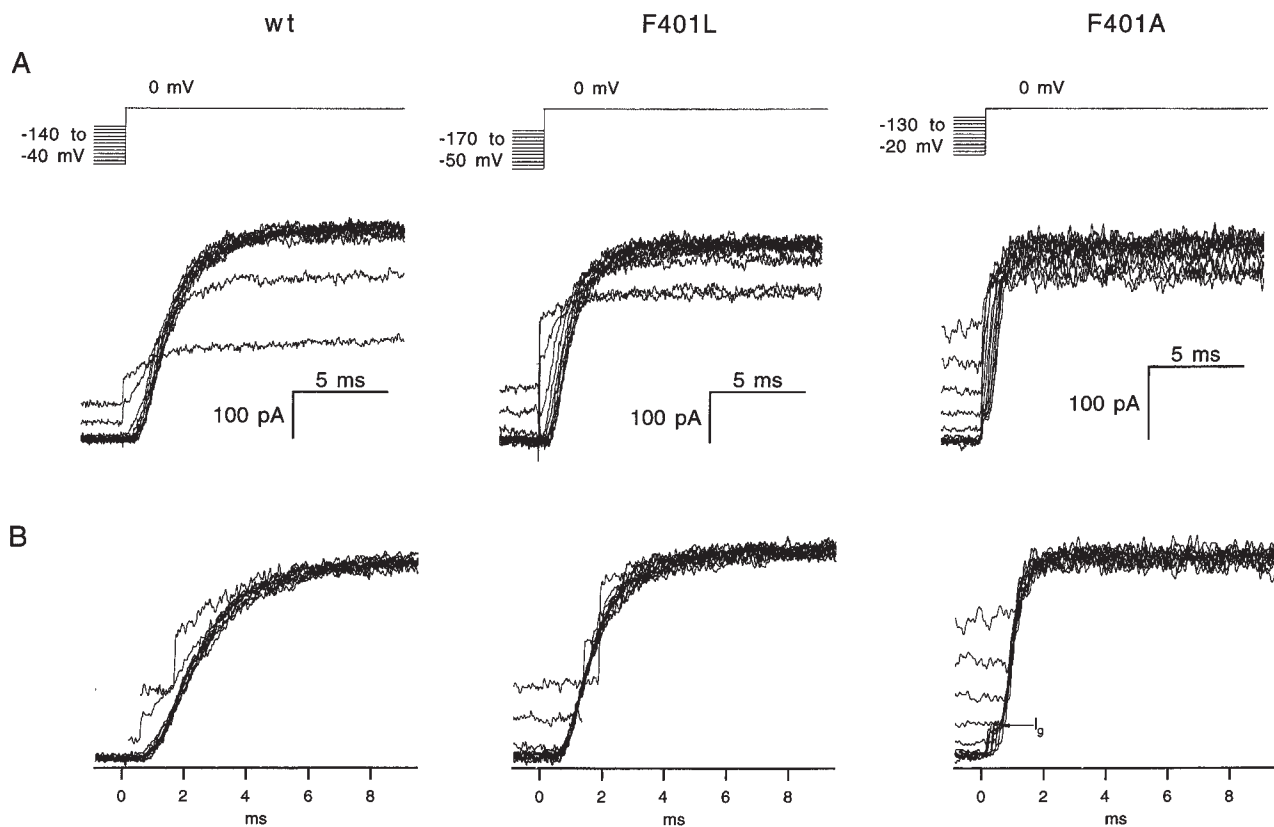


Figure 11. Mutations of F401 and cooperative gating: Cole-Moore analysis. (A) Families of currents from the wt, F401L, and F401A channels were obtained as follows: pulses to 0 mV were preceded by 1-s-long prepulses to voltages between –140 and –40 mV (wt, left), –170 and –50 mV (F401L, center), or between –130 and –20 mV (F401A, right). A few of the most depolarizing prepulses are in the activation range of the channels, as evident from the steady current recorded during the prepulse. The most negative prepulses induce greatest delay at the onset of activation. (B) The voltage families above were scaled in amplitude to match at the peak to compensate for steady state C-type inactivation incurred at the more depolarized prepulses. Scaled traces were then shifted along the time axis to obtain the best superposition. Note that, whereas in wt and F401L (left, center) traces in which the prepulse opens channels with detectable probability are not superimposable on the rest of the family, in F401A such behavior is not seen. At the onset of current during the main pulse, gating currents can be seen as bumps in the F401A family.

on the rest of the family by this procedure (Fig. 11 B, left; Zagotta et al., 1994a). This property is also observed with F401L channels (Fig. 11, middle). In contrast, in F401A, the Cole-Moore shift is present with complete superimposability over the prepulse voltage range of -130 to -20 mV (Fig. 11, right). During the more depolarized prepulses in this family, F401A channels are significantly activated, but their entry into the open state confers no new kinetic features to the 0-mV traces that would suggest nonindependent subunit behavior.

Gating Charge Movement Reveals Stability of the Open Conformation

Kinetics of the return of gating charge (I_g^{OFF}) upon stepping from a positive to a negative voltage provide important information about the voltage-dependent reverse transitions (those leading away from the open state). In potassium channels, their dependence on the duration and amplitude of the preceding depolarization has been extensively studied (Bezanilla et al., 1991; Perozo et al., 1992, 1993; Bezanilla et al., 1994; McCormack et al., 1994; Zagotta et al., 1994b; Hurst et al., 1997; Schoppa and Sigworth, 1998c). In *Shaker*, the time course of gating charge return at the end of a voltage pulse depends strongly on the voltage and duration of the depolarization. After depolarizing steps to negative voltages that would result in a low probability of channel opening, gating charge return follows a rapid nearly exponential time course, reflecting redistribution of channels among closed states. At more positive test voltages, increased pulse durations give rise to I_g^{OFF} that is characterized by a rising phase and a slowly decaying time course. This observation fits with the idea that channels entering the open state leave it only slowly, "trapping" charged domains in the activated conformation.

Fig. 12 A contrasts the effect of test-pulse duration at three voltage levels on I_g^{OFF} in wf, wF401L, and wF401A channels. With pulses to -50 mV, charge return upon repolarization to -100 mV remains rapid in wf and wF401A for pulse durations between 1 and 57 ms (wf) and 41 ms (wF401A). F401L channels are significantly open at this voltage, however, and the OFF gating currents in wF401L accordingly display progressively diminished amplitude and a prolonged declining phase as pulse length exceeds ~ 3 ms. A pulse amplitude of -30 mV (Fig. 12 A, middle left) marks a transition zone for the kinetics of the wf I_g^{OFF} . Pulses of a few milliseconds duration do not impede subsequent rapid charge return, those longer than ~ 10 ms give rise to OFF currents with complex time courses in which at least three kinetic components can be recognized, and those >25 ms produce a rising phase and exponential decay. wF401L OFF gating currents with all but the shortest -30 mV pulses are notable for the greatly

slowed charge return that is incomplete after up to 30 ms at -100 mV (Fig. 12 A, middle center). The families of wf and wF401L channels show progression of the same trends when the pulse amplitude is 0 mV. In fact, I_g^{OFF} becomes nearly "immobilized" in wF401L, displaying protracted decay after pulses lasting longer than 3–4 ms.

wF401A gating currents are unlike those of the other two species. With pulses to 0 and $+100$ mV, the latter of which are sufficient to activate many F401A channels, the time course of the OFF currents is rapid and unaffected by pulse length (Fig. 12 A, right). The small steady state outward current seen at $+100$ mV is an ionic current contaminant, likely of native *Xenopus* oocyte origin because its appearance at that voltage is variable among different cells and does not depend on the level of channel expression. Its tail current also accounts for a very small slow phase on the OFF gating currents after longer pulse durations. The results for the wf (left), wF401L (center), and wF401A (right) channels are summarized in Fig. 12 B, which plots the time constants from exponential fits to the decaying phase of I_g^{OFF} as a function of the length of pulses at the different pulse voltages. The time course of the OFF gating currents has a complex waveform, and these single-exponential fits are not meant to imply that there is an underlying first-order kinetic process; rather, they provide a ready means to document a transition from a predominantly fast to a slow process. For wF401A, they additionally illustrate that as the probability of channel opening is changing over a voltage range of 150 mV, the kinetics of charge return at -100 mV are barely altered.

Kinetic Mechanisms for Nonindependent Gating

Ionic and gating current results described in the preceding section imply that mutating phenylalanine to alanine at position 401 drastically diminishes the cooperative stabilization of the open state characteristic of the wild type, whereas the leucine mutation augments it. In the following, we investigate this hypothesis quantitatively, using kinetic principles and models previously developed for *Shaker* gating.

Several general features of *Shaker* gating have been established by diverse means in different laboratories (e.g., Bezanilla and Stefani, 1994; Sigg et al., 1994; Sigworth, 1994; Zagotta et al., 1994a,b; Aggarwal and MacKinnon, 1996; Baker et al., 1998; Schoppa and Sigworth, 1998a,c). These include: (a) activation is a multi-step process involving more than a single transition per subunit, (b) activation requires the translocation of ~ 14 elementary charges across the electrical field of the membrane, (c) charge movement is spread over a number of transitions and its quantity is not the same for all transitions, (d) for most transitions toward

the open state, more charge moves after the transition state than before it, (e) some of the transitions late in activation carry a greater amount of charge than the earlier transitions, (f) gating among closed states can be approximated by independent action of the subunits, (g) open channels can close to states that were not necessarily traversed during the activation process, (h) transitions that involve the open state disobey the predictions of subunit independence.

One relatively simple formalism that has been put forth to account for these features of gating is the scheme of Zagotta et al. (1994b), which will be referred to as the ZHA model, which explicitly introduces a cooperative factor θ by which the first closing transition rate is divided. Otherwise, the activation pathway in this model is an independent process involving four gating subunits, each undergoing two sequential charge-moving transitions. The ZHA model is shown in an abbreviated form in Fig. 13 A, emphasizing the fourfold symmetry. We used the parameters of the original ZHA model (Zagotta et al., 1994b) to simulate the G(V) (Fig. 13 B), ionic currents for steps to +50 mV followed by a tail voltage of -65 mV (Fig. 13 C), steady state charge-voltage relation [Q(V)] (Fig. 13 D), and the dependence of the time course of the OFF gating currents on the duration of -30-mV pulses (Fig. 13 E). In each case, the variable parameter was the factor θ , which was either 1, 9.4, or 50. These were chosen to give the best overall approximations of the F401A, wt, and F401L channels' behavior, respectively. For F401A, the cooperativity factor (θ) was set to a value of 1, the equivalent of complete subunit independence. The model succeeds in correctly describing the order of relative steepness of the G(V) curves, of the deactivation kinetics, and of the duration dependence of I_g^{OFF} . However, the extremely shallow voltage dependence of F401A channel opening (Fig. 5) could not be reproduced by the model, even with the introduction of a modest amount of negative cooperativity ($\theta = 0.4$; Fig. 13 B).

The ZHA model provided a convenient starting point for arriving at kinetic descriptions of the wt and mutant currents. Manipulating only the degree of cooperative slowing of the first closing transition with changes to the factor θ does surprisingly well in describing the basic properties of the F401 mutant channels. However, the model proves inadequate for the quantitative agreement with the macroscopic ionic and gating current data. Proper fits to the kinetics of channel opening, steady state G(V) relations, ON gating currents, and the steady state Q(V) curves all require manipulation of additional parameters of the ZHA model and in a number of cases were unattainable without altering the fourfold symmetric structure that had made it so conceptually attractive. Therefore, we broadened our consideration of candidate models to include ones where a

separate concerted transition (or transitions) connects the four parallel and independent activation pathways (one per subunit) to the open state. Precedents for this mechanism can be found in earlier models for potassium channels (Koren et al., 1990; Zagotta and Aldrich, 1990a; Schoppa and Sigworth, 1998c; Ledwell and Aldrich, 1999). This class of models provides the conceptual advantage of preserving the symmetric nature of the activation pathway while introducing only a few additional free parameters compared with the model of Zagotta et al. (1994b) and Smith-Maxwell et al. (1998b).

A detailed kinetic model of this class has been proposed for *Shaker* and a mutant channel (V2) (Schoppa and Sigworth, 1998c), which argues for the necessity to include a third charge-translocating step per subunit as well as two sequential concerted transitions preceding channel opening (a so-called 3+2' scheme). We opted for the simpler (2+1') model because of the limited experimental means to constrain a more elaborate scheme for all three channel species in this study. Our goal is to provide a robust description of the main aspects of the channels' gating while minimizing the number of transitions that differ among the models for the wt, F401L, and F401A channels. Our ability to do so supports the hypothesis that F401 mutations do not disrupt the wt gating mechanism in a global sense, but only target specific aspects of it. Our model provides reasonable fits to the wt and mutant channels, with major differences among the three species primarily limited to the first closing transition, as suggested by our data and the predictions of the original ZHA model (Fig. 13). Fig. 14 shows the connectivity of the model and illustrates that despite the large number (17) of kinetic states, only 12 free parameters are needed to constrain the mechanism up to and including the concerted Closed \leftrightarrow Open transition, compared with 9 for the ZHA model and 20 for the 3+2' model of Schoppa and Sigworth (1998c). These are the zero-voltage rate (k_0) and associated valence (z_k) of the two forward rates α and γ and the two reverse rates β and δ for each of the four subunits and of the forward rate κ and the reverse rate λ for the concerted transition. The rates are assumed to be instantaneous exponential functions of voltage, according to:

$$k = k_0 e^{z_k FV/RT}$$

The total charge displacement for each channel is constrained to be $\sim 14 e_0$ (14.47 e_0 for the wt, 14.37 e_0 for F401A, and 14.07 e_0 for F401L), in agreement with previously published measurements in wt (Aggarwal and MacKinnon, 1996; Noceti et al., 1996; Seoh et al., 1996; Schoppa et al., 1992).

Kinetic transitions that follow channel opening at depolarized potentials are to states that are not obligato-

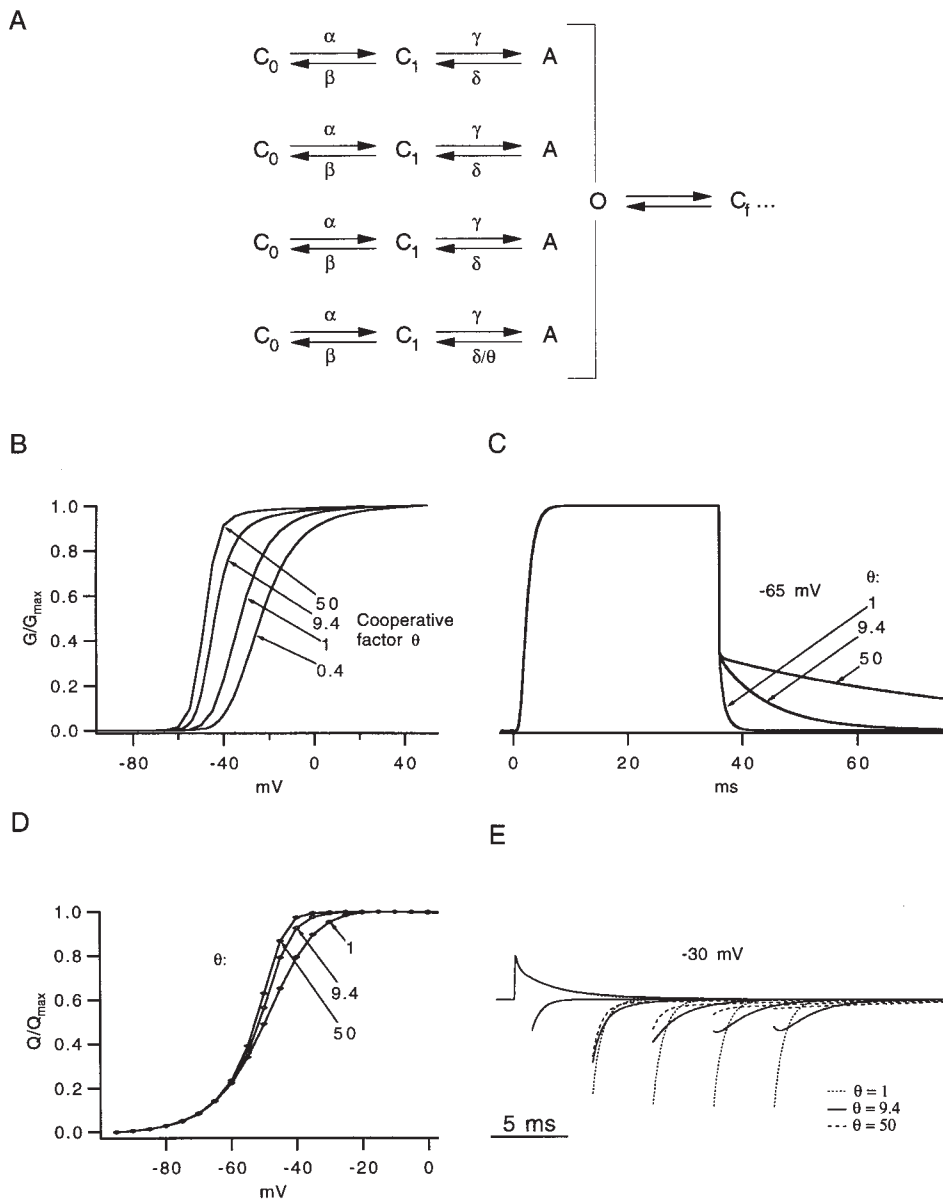


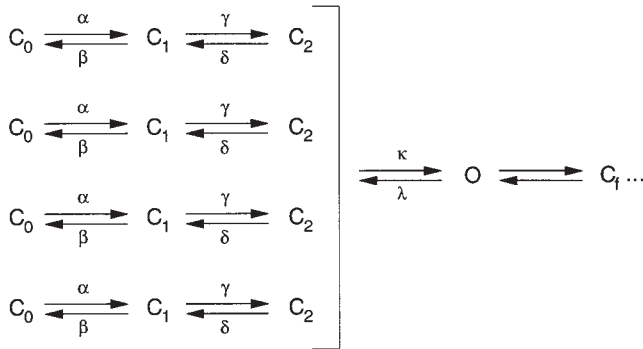
Figure 13. Predictions of the ZHA model at different levels of cooperativity. (A) Connectivity of the ZHA model is shown in the collapsed format (for expanded version showing all nondegenerate states, see Fig. 7 of Zagotta et al., 1994b). Note that the rate of the first backward transition for leaving the open state is slowed by the cooperative factor θ . Simulations were performed on the versions of the ZHA model that varied the value of the factor θ as indicated. Simulated currents were then analyzed in the manner identical to the experimental data. Shown are the simulations for the normalized steady state $G(V)$ relationship (B), ionic tail currents at -65 mV (C), normalized steady state $Q(V)$ relation (D), and pulse-length dependence of the OFF gating current at -30 mV (E).

rily traversed during the activation process. These have been characterized using single-channel recordings of wt *Shaker* (Hoshi et al., 1994; Schoppa and Sigworth, 1998a). The predominant fast component of closed durations seen at depolarized voltage can be accounted for by including a state (shown as $C_{f...}$ in Fig. 14, top) that channels can enter after opening by a nearly voltage-independent transition. For our modeling of wt, we used the rate parameters for this transition given in Zagotta et al. (1994b). Because the open single F401A channels tend to have very brief flickery openings that are incompletely resolved in our records, we were unable to conduct quantitative analysis of the open and closed durations for this mutant and, therefore, lack the basis for detailed comparison with the wt data. We chose to assign the wt values for the $O \leftrightarrow C_{f...}$ transi-

tion to the same values in all three channel species rather than let them vary among the wt, F401L, and F401A.

Testing Model Predictions in wt and Mutant *Shaker* Channels

Fig. 15 A shows the fits of the model shown in Fig. 14 for the wt, wfF401L, and wfF401A channel's steady state charge vs. voltage curves. Equilibrium constants for the two charge-moving transitions in each subunit and for the concerted step were optimized to obtain the desired steepness and position along the voltage axis. The total charge displacement for a given transition is the sum of the charges that move before and after the transition state or, equivalently, that are associated with the forward and backward rates of that transition. The



k	wt		F401L		F401A	
	k_0	z_k	k_0	z_k	k_0	z_k
α	560	0.25	950	0.25	1050	0.25
β	184	1.1	153	1.0	184	1.0
γ	1340	0.8	3219	0.8	3219	0.9
δ	15	1.2	13.1	1.2	13	1.2
κ	5000	0.3	5000	0.3	5000	0.3
λ	91	0.6	40	0.6	10000	0.5
$O \rightarrow C_f \dots$	600	0	600	0	600	0
$C_f \dots \rightarrow O$	3800	0.17	3800	0.17	3800	0.17

Figure 14. A kinetic model for *Shaker* and the F401 mutants. Note that, compared with the ZHA model, independent transitions within each of the four subunits are completely symmetrical and that a concerted transition precedes channel opening. A closed state in which all four subunits are in the C_2 state is implicit in the model; it is referred to as the C_n state in the text. (Bottom) The model estimates of the zero-voltage rate constants (k_0 , in s^{-1}) and associated quantities of charge movement (z_k , in e_0) for each of the rates for the wt, F401L, and F401A channels are shown. The initial closing transition parameters are enclosed in a box to highlight the differences among the models.

three channels differ the most in their equilibria for the concerted opening transition. The zero-voltage equilibrium constants for this step are 55, 125, and 0.5 for the wf, wF401L, and wF401A, respectively. The marked decrease in wF401A provides part of the explanation for the shallowness of the slope of its $Q(V)$ curve, even though this transition carries only $\sim 1/16$ of the total charge displacement in the channel. To describe accurately the relatively shallow lower portion of each of the curves, it is necessary to make the charge displacement associated with the second of the two sequential subunit transitions ($z_{\gamma\delta}$) greater than that of the first ($z_{\alpha\beta}$) (Bezanilla et al., 1994). For all channel

species, the quantity $z_{\gamma\delta}$ is 2.0–2.1 e_0 . The first transition carries the charge of 1.35 e_0 . Models for wF401L and wF401A channels make the zero-voltage equilibrium constant for the first transition,

$$K_{0\alpha\beta} = \frac{k_{0\alpha}}{k_{0\beta}},$$

approximately twice as great, and that for the second transition,

$$K_{0\gamma\delta} = \frac{k_{0\gamma}}{k_{0\delta}},$$

nearly three times as great as those of the wf model in order to account for the more negative voltage range over which the initial gating charge movement occurs in the mutants.

In Fig. 15 B, model fits are shown superimposed on families of gating currents. The fits are a good description of the time course of I_g^{ON} obtained at depolarized voltages and of the I_g^{OFF} . However, the models predict too rapid a rise and decay of the ON gating currents in the activating voltage range (approximately -80 to -40 mV for all three channels). The data suggest the presence of a rising phase in the I_g^{ON} records even at these negative voltages. We were able to qualitatively improve on these fits by introducing a three-step per subunit activation sequence after Schoppa and Sigworth (1998c), but this approach was not pursued further as discussed above. The time course of the decay phase of the I_g^{ON} at depolarized voltages is a reflection predominantly of the forward rates of charge-moving transitions among closed states. Fitting single-exponential functions to I_g^{ON} at 0 mV provides a way to estimate a weighted average of the rates α_0 and γ_0 . The wf time constant from such fits is ~ 2.5 ms ($n = 11$), which is over two times greater than the time constants for wF401L and wF401A. This provides the rationale for assigning the values of $\alpha_0 = 560$ s^{-1} and $\gamma_0 = 1,340$ s^{-1} for wt, or about one half of the corresponding zero-voltage rates for the two mutants. As described earlier, the kinetics of I_g^{OFF} are very sensitive to the amplitude of the voltage step in the wf and especially wF401L, but not in wF401A. The model is able, by the large differences in the first closing rate λ , to account for the time course of the OFF gating current in the three families.

Inspection of the time course of the gating charge return as a function of pulse duration (Fig. 12) reveals important differences among the three channel species. Model fits to these data, shown in Fig. 16, indicate that our simulations are adequate to describe the time course of I_g^{OFF} for a variety of pulse durations at -50 and 0 mV. In particular, the observed slow decay of OFF gating currents observed in wF401L at -50 mV at longer pulse durations as the consequence of significant open probability of the channels at that voltage is

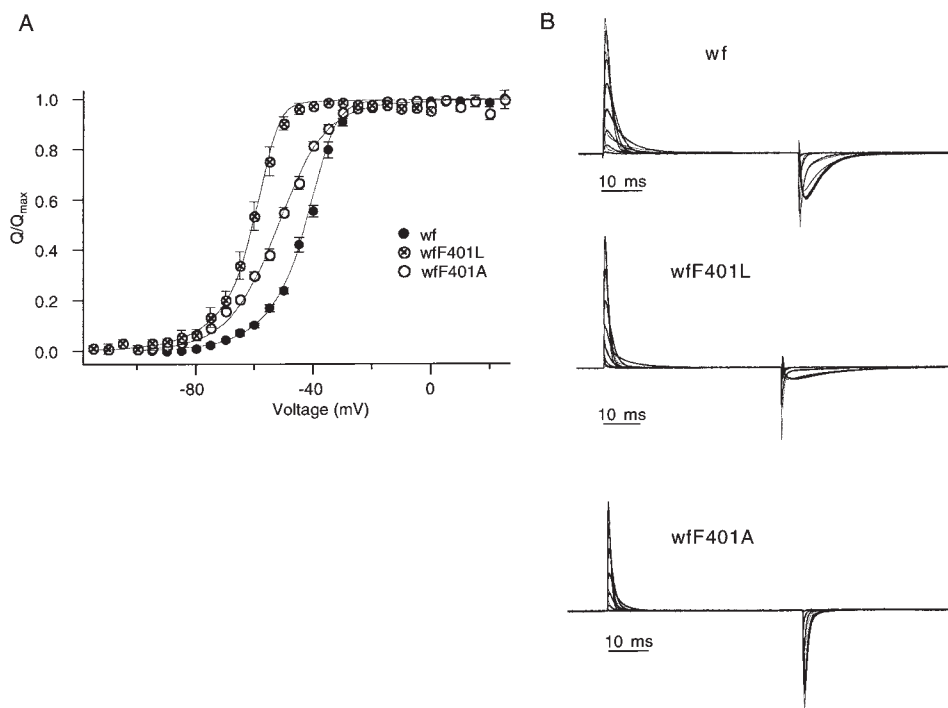


Figure 15. (A) Model description of the steady state gating charge movement. The averaged $Q(V)$ curves for the wf, wfF401L, and wfF401A channels are replotted from Fig. 9. Fits of the model in Fig. 14 are shown superimposed as solid lines. These were obtained by integrating the simulated OFF gating currents at -100 mV, low-pass filtered at 10 kHz, following steps to the test potentials shown on the x axis in 2-mV increments and normalizing by the charge obtained at the most positive voltages. This analysis follows the normal procedure we use for the experimental data. (B) Comparison of gating current kinetics with the model predictions. Representative families of gating currents from oocytes containing wf (top, from -80 to $+40$ mV), wfF401L (middle, -80 to $+40$ mV), and wfF401A (bottom, -95 to $+25$ mV) channels are shown. Voltage increment is 20 mV in

each case. Simulated gating currents are superimposed (thin lines). Models shown in Fig. 14 were used for the three channels, with the following modifications to obtain better fits to these experimental families: in the wf model, $\lambda_0 = 101$ s $^{-1}$; in the F401L model, $\lambda_0 = 39$ s $^{-1}$; and in the F401A model, $\kappa_0 = 3,500$ s $^{-1}$, $\lambda_0 = 8,000$ s $^{-1}$, and $z_\gamma = 0.8$ e_0 .

observed in simulated traces. The complex waveform of wf I_{g}^{OFF} after 0-mV pulses lasting ~ 10 ms deviates somewhat from the predictions of our model and would probably be better fit with the introduction of additional steps in the activation pathway (see above). The model predicts that the gating charge return will be rapid and independent of pulse duration in wfF401A, which is clearly a feature of our data.

The predictions of the models for the macroscopic ionic currents are shown in Fig. 17. Representative families of activating currents recorded from patches containing wt, F401L, and F401A channels are qualitatively comparable to model simulations at matching voltages in terms of the overall sigmoidal character and the voltage range over which activation kinetics are most noticeably changing. A consistent finding for all three channels is that the model traces appear to have a slower overall time course than the patch data. This discrepancy is quantified in Fig. 17 B, which displays model predictions for the time constant of activation derived from fitting the late phase of current time course (Zagotta et al., 1994a) and in Fig. 17 C in which the time-to-half-maximum current is plotted for the three models. The relative order of magnitudes of experimentally derived values for the three channels are preserved in the model simulations. While a shift of approximately -10 mV between the model and data results in closer agreement, these kinetic measurements

obtained in excised inside- and outside-out patches are not easily superimposable on the model simulations by a simple voltage offset. We wondered if the model parameters that are mostly determined using gating current recordings obtained with cut-open oocyte clamp systematically predict slower ionic currents as the result of differences inherent in the two recording techniques. Stefani et al. (1994) demonstrated that for the kinetics of gating currents, the cut-open oocyte clamp technique produced very similar results to those obtained with cell-attached macropatches. In our experience, activation kinetics of *Shaker* in cell-attached patches are somewhat slower (and deactivation is faster) than the excised patches we used. We elected not to alter the models extensively to try to accommodate both the cut-open oocyte clamp and excised patch data sets, but instead focused on qualitative agreement between experimental ionic current results and model simulations.

In evaluating model predictions for the steady state open probability vs. voltage, we took notice of the observed differences in the voltage positions of $G(V)$ curves obtained using wt cell-attached and excised patches. The former tended to be shifted positively by ~ 6 mV (data not shown). When displaying the $G(V)$ curves for wt, F401L, and F401A with their respective models in Fig. 18, we similarly offset the simulated curves by between -6 and -7 mV to compare them

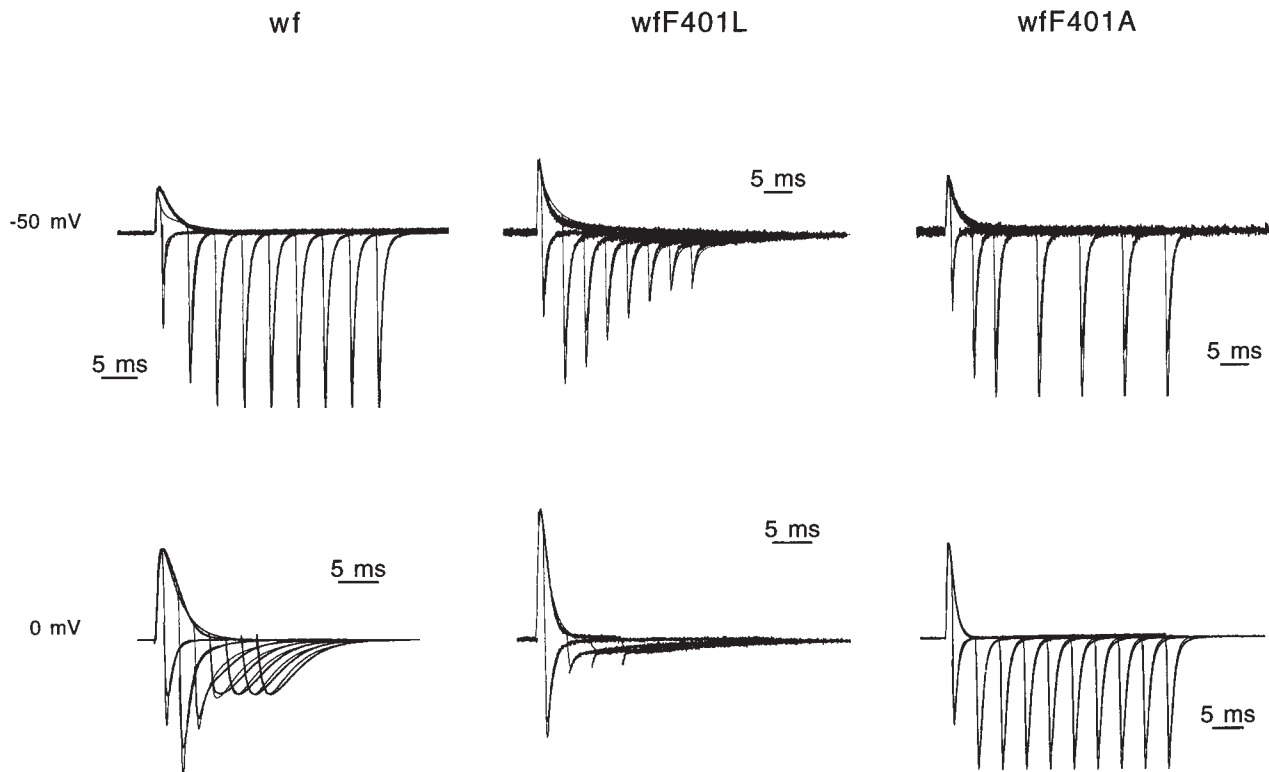


Figure 16. Model predictions for the pulse duration dependence of the OFF gating charge movement. Experimental records of wf (left), wfF401L (center), and wfF401A (right) gating currents obtained at -50 and 0 mV are shown as in Fig. 12. The fits of the corresponding models are shown overlaid (thin lines). Modifications of the models needed for these simulations were as follows (s^{-1}): for wf, $\beta_0 = 153$, $\delta_0 = 14$, and $\lambda_0 = 113$ at 0 mV; for wfF401L, $\alpha_0 = 1,150$, $\delta_0 = 11.5$, and $\lambda_0 = 39$ at -50 mV and $\beta_0 = 136$ and $\delta_0 = 11.5$ at 0 mV; and for wfF401A, $\alpha_0 = 1,200$ and $\lambda_0 = 8,000$ at both -50 and 0 mV.

with the experimental results. With this correction, both the steepness and the midpoint of the voltage dependence for wt and F401L channels were well described by the model. As earlier, the shallowness of the $G(V)$ relation in the F401A mutant precludes us from observing saturation of the open probability within the attainable voltage range. Therefore we cannot meaningfully normalize $G(V)$ data from different patches for direct comparison. Instead, $G(V)$ relations from a representative F401A patch obtained by two means [isochronal tail $G(V)$ and pulse $G(V)$] are shown in Fig. 18. Model traces for F401A were analyzed in the analogous manner, and the resulting $G(V)$ curves are shown scaled to match F401A curves at $+100$ mV after a -6 -mV shift along the x axis. The model, which postulates that the extremely shallow $G(V)$ curve results from a destabilization of the open state by greatly speeding the initial closing transition, is qualitatively supported by these data.

The proposed alterations in a backward transition leading away from the open state are expected to affect the time course of macroscopic ionic tail currents. Fig. 19 (top) shows, for the wt and the two F401 mutants, the decay in the relative open probability as a function of time when voltage is stepped from a depolarized

value of $+50$ mV to hyperpolarized potentials. All current traces are normalized to match their initial amplitudes. In Fig. 19 (bottom), these data are re-plotted on a logarithmic time axis. These two transformations allow a closer examination of the kinetics of deactivation at the more hyperpolarized voltages at which tail currents are very small and rapid. Additionally, a logarithmic time scale would bring out the convergence of the open probability traces to an asymptotic value at very low voltages if a single closing transition were to become rate limiting. We used the models for the wt and F401L in which initial closing rates were modified somewhat to reflect the slower deactivation kinetics in excised patches. With λ_0 set to $50 s^{-1}$ for the wt and $29 s^{-1}$ for F401L, the open probability decay is well described by the model predictions for both channels over the range -60 to -160 mV (-180 mV for F401L). The valence of $0.6 e_0$ assigned to this rate is the minimum required to produce the necessary spacing of the traces at voltages below -120 mV (Fig. 19, bottom). Less charge associated with the first closing step predicts a rate-limiting step that is not evident in the data. The analysis of F401A deactivation (Fig. 19, right) is complicated by the extreme rapidity of its tail currents

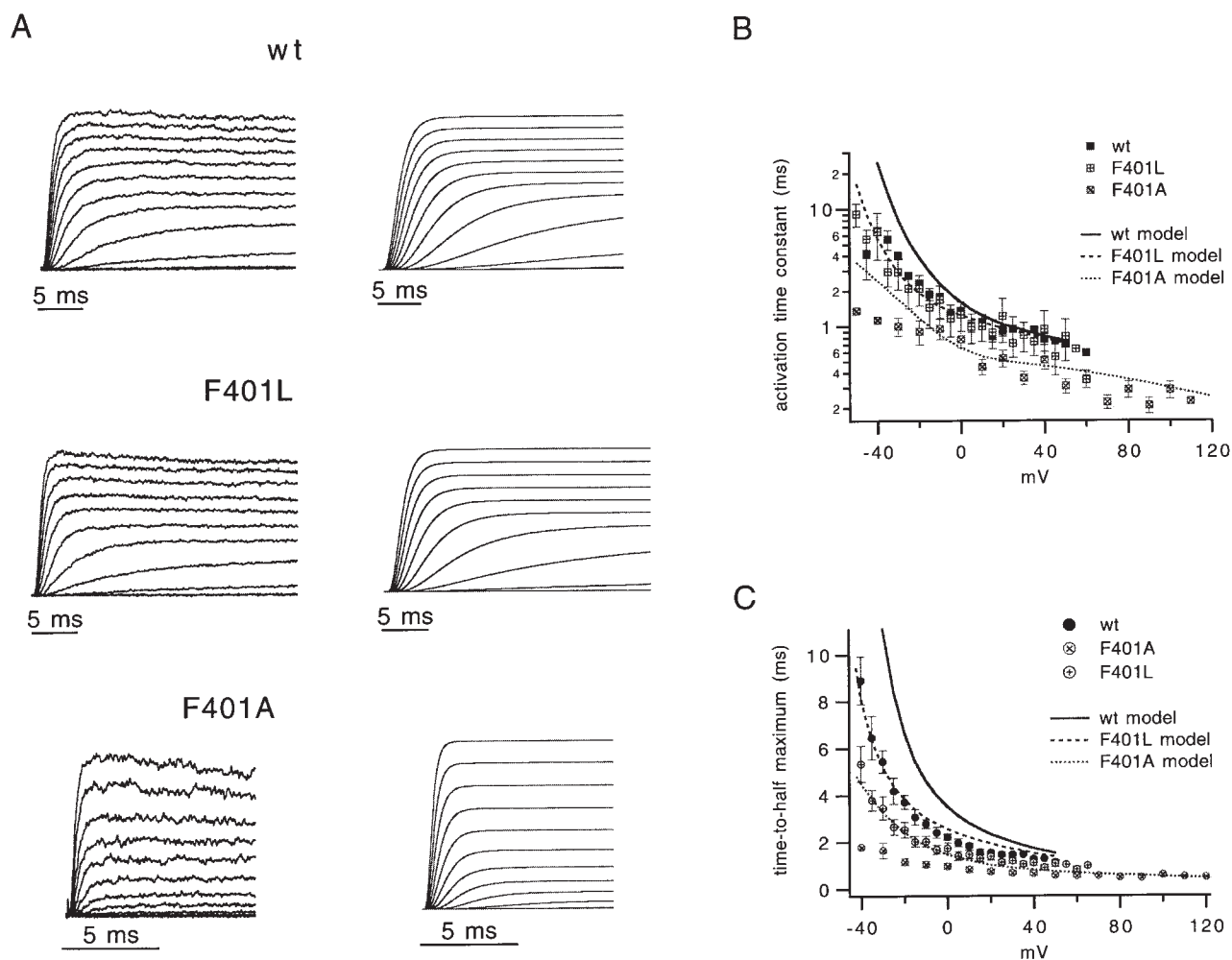


Figure 17. (A) Model predictions for the activation of ionic currents. On the left, representative families of currents recorded at between -90 and $+50$ mV (wt), -95 to $+25$ mV (F401L), and -80 to $+140$ mV (F401A) are displayed. Voltage increments were 10 mV (20 mV for F401A). Corresponding simulated ionic currents are shown on the right. Model parameters were not altered from those in Fig. 14, B and C. Comparison of the model with measured ionic current activation kinetics. Activation time constants (B) and time-to-half-maximum (C), obtained as described in the text, are plotted as a function of test voltage for wt, F401L, and F401A channels. Predictions of the models are shown as solid and dashed lines. These were obtained by the same analysis procedures applied to the simulated currents as to the experimental records.

over a wide voltage range. Fitting exponential functions to their time course yields time constants in the range of 100 – 500 μ s, which are difficult to resolve well when the current amplitudes are small. Additionally, there is a prominent component of OFF gating current (note the lowermost trace in the panel which was taken at -90 mV) that is slower than the ionic tail in this mutant and significantly distorts its kinetics. Simulated F401A traces have a multi-exponential decay, with the very rapid component near the limit of resolution in our recordings (and perhaps more rapid than the excised patch data), and a slower component that at -30 and -50 mV cannot be reliably distinguished from the steady state component seen in the experimental data. Because of the nonionic components of the current de-

cay (which the model does not take into account), more detailed comparison of the model simulations to the tail currents in F401A at hyperpolarized voltages was not undertaken.

Sigmoidal activation kinetics are a cardinal feature of *Shaker* channel gating and, as shown in Fig. 10, they remain present in the F401 mutants. The amount of sigmoidicity, as defined earlier, and the way it varies with pulse potential is a sensitive means to assess the presence of a slow first reverse transition from the open state (Zagotta et al., 1994a). In Fig. 20, the models for the wt, F401L, and F401A that differ mainly in the rate of that transition are used to generate activation families that are scaled in amplitude and time, as described in the discussion of Fig. 10. The relative spacing of

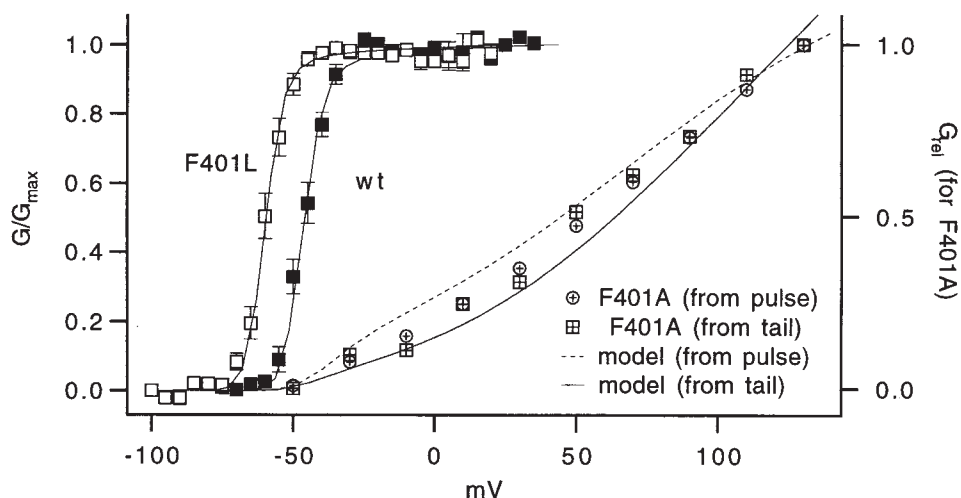


Figure 18. Model description of the conductance-voltage relationships. Experimental data for wt, F401L, and F401A are shown plotted as in Figs. 1 and 5. Simulated $G(V)$ relations were generated from current families taken every 2 mV. The resultant curves were then shifted negatively by 6 (wt and F401L) or 7 (F401A) mV and shown superimposed as lines. The predicted $G(V)$ curves from pulse and tail (see methods) for F401A were normalized to match the maximum relative conductance of the data.

these traces gives a measure of sigmoidicity over the voltage ranges of -35 to $+55$ mV (wt model), -55 to $+45$ mV (F401L model), and -40 to $+120$ mV (F401A model). As in the experimental records, F401L and wt

model simulations show the progression from lower to asymptotically higher sigmoidicity, which is a prediction for a forward biased cooperative step with the slow rate of leaving the open state. F401A simulations dis-

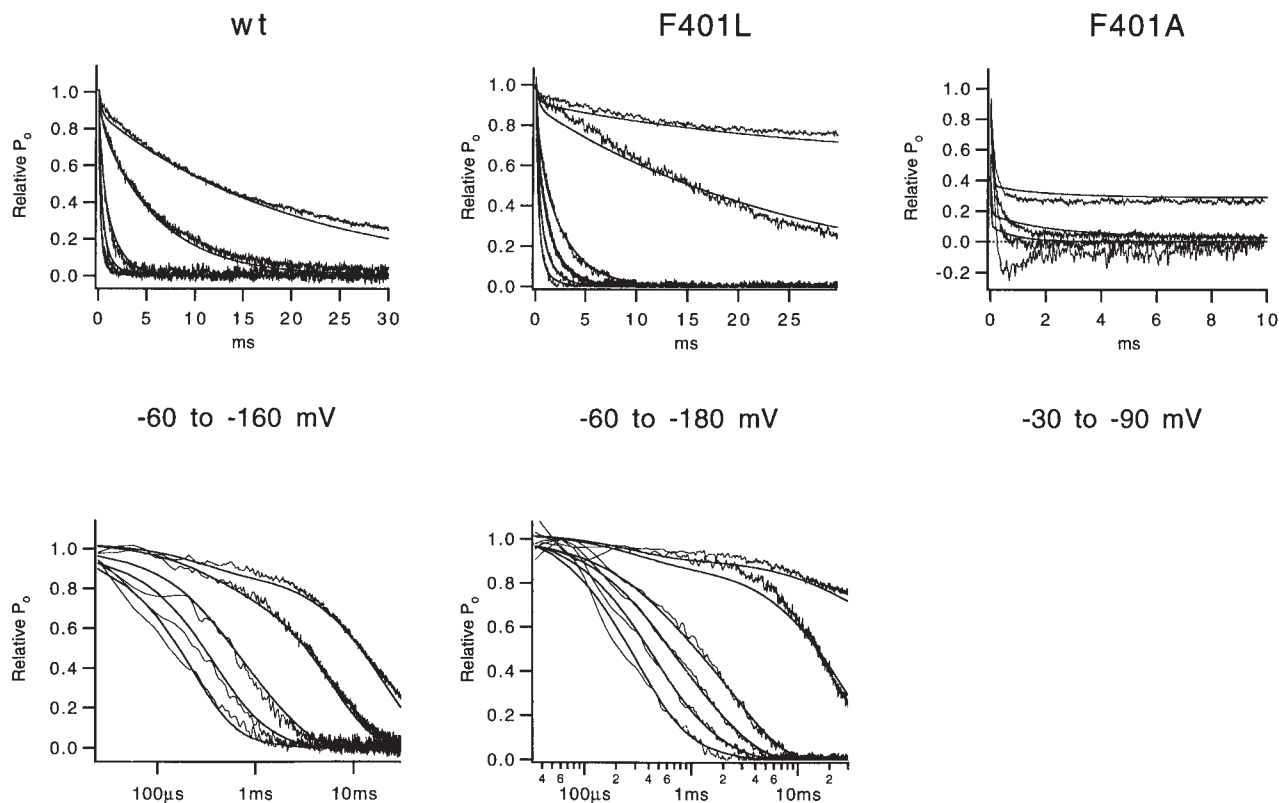


Figure 19. Models predict the deactivation kinetics in *Shaker* and F401 mutants. Ionic tail currents that arise during channel deactivation at negative voltages are shown as relative open probability as the function of time by scaling to match the instantaneous amplitudes after the end of the $+50$ -mV test pulse (top). The current families for the tail voltages of -60 to -160 mV (wt, left), -60 to -180 mV (F401L, center), and -30 to -90 mV (F401A, right) are shown. Records at -100 mV are omitted because the current amplitudes are very low near the reversal potential. Note the inward current at the start of the tail at -90 mV in F401A, which is largely due to the OFF gating current component. Model predictions for the time course of the open probability decay are superimposed as thin lines. (Bottom) The data and model traces for the wt and F401L are replotted on a logarithmic time axis to enable closer comparison of the model to the data at the lowest voltages. For these simulations, λ_0 was 50 and 29 s^{-1} for the wt and F401L models, respectively.

play nearly identical sigmoidicity over a wide voltage range characteristic of this mutant's currents.

discussion

In this paper, we have confirmed, with direct evidence obtained from channels without N-type inactivation, the hypothesis put forth by Zagotta and Aldrich (1990b) that *Sb*⁵ (F401A) selectively reduced the voltage dependence of deactivation with little effects on the forward transitions. Any effects of *Sb*⁵ on inactivation can be most economically explained by the tight coupling of intrinsically weakly voltage-dependent inactivation to the altered activation process (Zagotta and Aldrich, 1990a,b).

We used F401, an important residue with known effects but a poorly understood mechanistic role in the activation process, as a molecular handle toward further elucidating the role of the S5 segment in gating. Progressively smaller aliphatic substitutions at this site produced more profound effects, with the important exception of leucine, as though the steric bulk of this residue is an important determinant of channel gating. A study of chimeras between Kv2.1 and Kv3.1 channels demonstrates that exchanging NH₂ terminus ends of S5 transfers differences in both deactivation of ionic currents and the OFF gating currents (Shieh et al., 1997). Based on our results comparing point substitutions of leucine and isoleucine, we believe that the differences can be attributed to the position equivalent to 401 in *Shaker* (position 332 in Kv2.1). Similar to our findings, Shieh et al. (1997) show that having an isoleucine at that site as part of a three amino acid chimeric substitution gives rise to fast deactivation gating, whereas a leucine-containing chimera is slow. Such profound consequences of a very conservative exchange of two bulky hydrophobic amino acids of identical molecular weight and van der Waals volume have precedents in potassium channels (Hurst et al., 1992; McCormack et al., 1993; Smith-Maxwell et al., 1998b) and in other proteins, particularly in their hydrophobic cores (Eriksson et al., 1993). These findings imply that the side chain of residue 401 occupies a sterically constrained space, likely interacting at close range with other amino acid residues in the channel. Alternatively, it is also worth noting that isoleucine is more similar to valine than to leucine with regard to its effects on the stiffness of the main chain in proteins. Because both isoleucine and valine branch at the β carbon atom rather than at the γ carbon, as is the case for leucine, their more proximal branch point limits the flexibility of the main chain backbone (Schulz and Schirmer, 1979). In our study, the similar behavior of the valine and isoleucine replacements at F401 and quite different behavior of channels with leucine at this position,

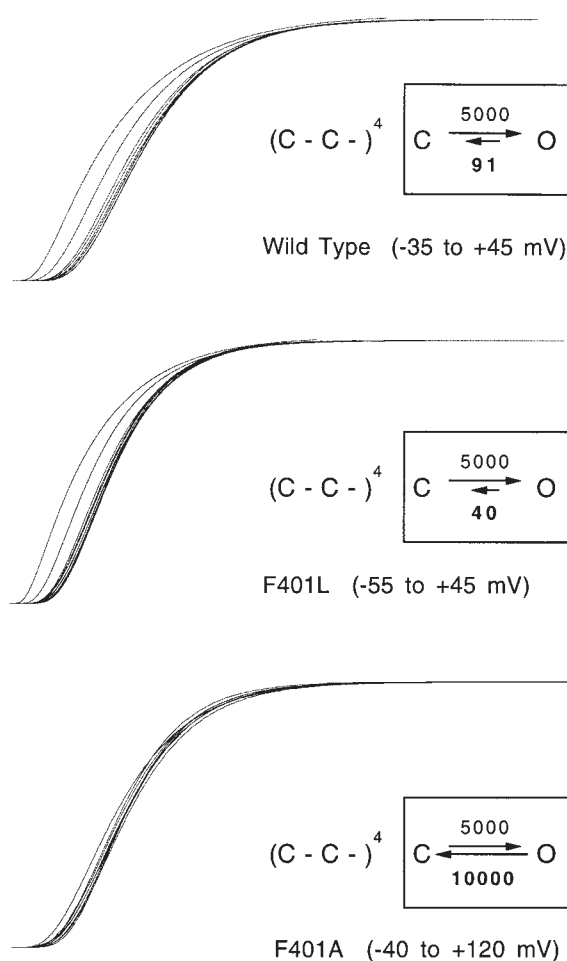


Figure 20. The model accounts for the sigmoidicity in wt and F401 mutants. The activation families for the three models, with the relevant transitions shown in the box, were scaled in time and amplitude as described in the text to assess the dependence of sigmoidal delay on pulse voltage. Current families were simulated at voltages shown. Compare these results with the experimental data in Fig. 10.

suggests perhaps that the ability of the main chain of the S5 sequence to bend as part of the gating conformational transitions may be important for the activation process.

The reduction in the apparent effective activating valence of the F401 mutations can be considered within the framework of several hypotheses: reduction in actual gating charge content, displacement of the voltage range over which some of the major charge-moving transitions take place, and altered coupling between a minor charge-moving transition intimately associated with channel opening and the rest of the activation pathway. Measurements of only steady state ionic currents are usually inadequate for distinguishing among these possibilities. Measurement of the limiting slope of activation (Almers, 1978), used for placing a lower limit on the gating charge, is usually unreliable unless it

is possible to resolve currents at very low open probability (Zagotta et al., 1994a; Sigg and Bezanilla, 1997).

With the aid of gating current recording, there are now two approaches available to count gating charges for testing the first hypothesis: one relies on ionic current fluctuation analysis (Schoppa et al., 1992; Noceti et al., 1996), and the other on quantitative binding of specific labeled toxin to the channel (Aggarwal and MacKinnon, 1996). Neither method has yet found an uncharged-for-uncharged mutation that would alter the gating charge content per channel measurement. In fact, the V2 mutation in *Shaker* (L382V) (McCormack et al., 1991, 1993; Schoppa et al., 1992; Schoppa and Sigworth, 1998b), which possesses wt charge content, is quite reminiscent of the F401A mutation in terms of its ionic and gating current kinetics. For these reasons, we considered a reduction in the gating charge content unlikely and gave priority to considering alternative hypotheses that do not invoke a reduction in the gating charge content in mutant channels.

An intriguing hypothesis for the role of F401 in wt gating is that the wt phenylalanine side chain is engaged in a cation-aromatic interaction with a basic amino acid in S4, reducing the energy penalty for having an unshielded gating charge buried in the membrane bilayer. While a few acidic residues in the S2 and S3 transmembrane segments appear to interact with some of the carboxy-terminus S4 basic amino acids, as indicated by second-site rescue mutations (Papazian et al., 1995), the abundance of aromatic amino acids in S5 presents an attractive possibility for stabilizing positive charges of the voltage sensor without forming strong electrostatic interactions.

In this light, the very fast gating behavior of the F401A single channel is similar to the published description of the charge-conserving S4 mutant R377K (Shao and Papazian, 1993). Amino acid sequence analysis suggests that these residues may be on adjacent putative alpha helices in proximity to the intracellular side of the membrane. At positive voltages, both mutations give rise to fast, flickery channel openings that are distinctly different from the wt phenotype. To explain the gating effects of F401 substitutions, we therefore considered the possibility that the phenylalanine at position 401 may interact specifically at close range with the potential gating charge R377. If that were the case, F401 could be stabilizing the otherwise unfavorable positive charge density of arginine at position 377 by a favorable π -electron ring-guanidinium interaction. This mechanism of stabilization also provides an explanation for the behavior of the lysine mutant at 377 (Shao and Papazian, 1993; Perozo et al., 1994), as this residue cannot enter into a favorable parallel stacking arrangement (Flocco and Mowbray, 1994) with an aromatic ring. Moreover, the F401A and R377K mutations might pro-

duce the similar observed single-channel phenotypes by disrupting different members of the interacting pair.

To explore this possibility further, we made a single point mutation, substituting a negatively charged glutamic acid at position 401 in the hope of observing effects of a salt bridge formation between it and R377. Also, we made a double mutant F401A-R377Q with the expectation that the small side chain bulk of alanine at position 401 might rescue the expression of R377Q currents by permitting the latter residue greater steric freedom. Neither construct gave rise to functional channels as detected by the ability to measure ionic currents. We cannot exclude the possibility that channel protein was made but did not undergo correct trafficking or cell membrane insertion. Therefore, the possibility of an S4 arginine-S5 aromatic interaction in gating remains an open question.

Upon initial inspection of the wt, F401A, and F401L ionic currents, their dissimilarities are quite striking. However, we observed considerable similarity among the channels in the movement of the gating charge among closed states at the low voltages where few channels open. Therefore, we sought to compare the properties of these channels that would be expected to change as the result of channel opening. Recent work on potassium channel gating mechanisms (Bezanilla et al., 1994; McCormack et al., 1994; Zagotta et al., 1994a,b; Schoppa and Sigworth, 1998a,c; Smith-Maxwell et al., 1998a,b) supports the idea that the final closed-to-open transition cannot be the result of activation of one of the four subunits independent of the others. Rather, a concerted change from one quaternary conformation of the channel to another has been envisioned. We tested the predictions of the independent model of activation for the three channels using the measurement of sigmoidicity (Zagotta et al., 1994a) and its dependence on holding potential (Cole and Moore, 1960; Moore and Young, 1981) and found that, for wt and F401L, the independent model failed when a significant proportion of the channels entered the open conformation. The change in sigmoidicity with voltage for these two channels was consistent with a relatively slow first closing step. In contrast, the F401A results conformed to an independent model or, alternatively, one in which the first closing transition is even faster than predicted by subunit independence. The movement of the returning gating charge was considerably slower in the wt and wfF401L (but not wfF401A) when the amplitude and duration of the voltage step were high enough to be expected to open many of the channels. Note that the gating current results are in line with the conclusions drawn from experiments with ionic currents, even though for the former we used a nonconducting version of the *Shaker* channel. This supports the idea that the determinants of open state stability are similar

whether or not there is macroscopic passage of permeant ions through the pore (see Chen et al., 1997).

Our model for the activation of *Shaker* and the two F401 mutations succeeds in describing a common gating mechanism. The differences in the models for the three channels are few and are limited, primarily, to the concerted opening transition. We can compare the effects of the mutations on the stability of the open conformation of the channel by calculating the free energy difference (ΔG) between the last closed state C_n and the open state from the rates of the final opening and first closing transitions in our model:

$$\Delta G(V) = -RT \ln \left[\frac{\kappa(V)}{\lambda(V)} \right].$$

The value of ΔG for the wt at 0 mV is -2.3 kcal/mol, which is increased to -2.8 kcal/mol by the F401L mutation. Correspondingly, both these channels are found overwhelmingly in the open state at 0 mV. The open state is, in contrast, less stable than the last closed state (C_n) by $+0.4$ kcal/mol in the F401A mutant. Therefore, the overall change in free energy difference ($\Delta\Delta G$) between these conformations resulting from the F401A mutation is 2.7 kcal/mol. However, since the F401A mutation is present in all four subunits of the channel protein involved in the concerted transition, considerations of symmetry lead us to conclude that four weaker interactions, each contributing ~ 0.7 kcal/mol to the open channel stability, are disrupted in the mutant channel. It is intriguing to consider the ener-

getic cost of the possible lost parallel stacking interactions between an aromatic ring and an S4 arginine side chain (Flocco and Mowbray, 1994) of the same or, possibly, adjacent subunits as one explanation accounting for the F401A results. An increase in open state stability conferred by the leucine substitution suggests that other physical factors, such as steric bulk, may be important as well.

The free energy difference between a channel in the open and next-to-open state could be greater than expected from independence because of a favorable binding interaction between a channel and permeant (or blocking) ions (Marchais and Marty, 1979; Swenson and Armstrong, 1981; Matteson and Swenson, 1986; Miller et al., 1987; Neyton and Miller, 1988; Spruce et al., 1989; Neyton and Pelleschi, 1991; Sala and Matteson, 1991; Demo and Yellen, 1992) or solvent molecules (Schauf and Bullock, 1979, 1980; Zimmerberg and Parsegian, 1986, 1987; Alicata et al., 1990; Zimmerberg et al., 1990; Rayner et al., 1992; Starkus et al., 1995). Whereas external rubidium ions slow deactivation in wt *Shaker* (Zagotta et al., 1994a), in F401A channels the fast closing kinetics are insensitive to this ion (Kanevsky, 1998). The use of deuterium oxide as external solvent also tends to slow the return of gating charge upon repolarization in the wt, but less so in the wfF401A mutant channels (Kanevsky, 1998). Thus, there is a suggestion for both of these mechanisms playing a role in open state stability that is disrupted by the F401A mutation.

We thank L. Toro for the kind gift of *Shaker* W434F high-expression vector, and T. Hoshi and D. Perkins for developing and perfecting modeling software. We acknowledge the help of C.A. Warren, J. Haab, and W.N. Zagotta in making several of the mutants. C.J. Smith-Maxwell and E.M. Ogielska made helpful comments on the manuscript, and Gargi Talukder helped with the figures.

M. Kanevsky was supported by Medical Scientist Training Program grant GM07365 from the National Institute of General Medical Sciences. R.W. Aldrich is an investigator with the Howard Hughes Medical Institute. This study was supported by the National Institutes of Health grant NS23294.

Submitted: 24 December 1998 Revised: 14 June 1999 Accepted: 15 June 1999

references

- Aggarwal, S.K., and R. MacKinnon. 1996. Contribution of the S4 segment to gating charge in the *Shaker* K⁺ channel. *Neuron*. 16: 1169–1177.
- Alicata, D.A., M.D. Rayner, and J.G. Starkus. 1990. Sodium channel activation mechanisms. Insights from deuterium oxide substitution. *Biophys. J.* 57:745–758.
- Almers, W. 1978. Gating currents and charge movements in excitable membranes. *Rev. Physiol. Biochem. Pharmacol.* 82:96–190.
- Baker, O.S., H.P. Larsson, L.M. Mannuzzu, and E.Y. Isacoff. 1998. Three transmembrane conformations and sequence-dependent displacement of the S4 domain in *Shaker* K⁺ channel gating. *Neuron*. 20:1283–1294.
- Bezanilla, F., E. Perozo, D.M. Papazian, and E. Stefani. 1991. Molecular basis of gating change in *Shaker* potassium channels. *Science*. 254:679–683.
- Bezanilla, F., E. Perozo, and E. Stefani. 1994. Gating of *Shaker* K⁺ channels: II. The components of gating currents and a model of channel activation. *Biophys. J.* 66:1011–1021.
- Bezanilla, F., and E. Stefani. 1994. Voltage-dependent gating of ionic channels. *Annu. Rev. Biophys. Biomol. Struct.* 23:819–846.
- Chen, F.S., D. Steele, and D. Fedida. 1997. Allosteric effects of permeating cations on gating currents during K⁺ channel deactivation. *J. Gen. Physiol.* 110:87–100.
- Cole, K.S., and J.W. Moore. 1960. Potassium ion current in the squid giant axon: dynamic characteristic. *Biophys. J.* 1:1–14.
- Demo, S.D., and G. Yellen. 1992. Ion effects on gating of the Ca⁽²⁺⁾.

- activated K⁺ channel correlate with occupancy of the pore. *Biophys. J.* 61:639–648.
- Doyle, D.A., J.M. Cabral, R.A. Pfuetzner, A. Kuo, J.M. Gulbis, S.L. Cohen, B.T. Chait, and R. MacKinnon. 1998. The structure of the potassium channel: molecular basis of K⁺ conduction and selectivity. *Science*. 280:69–77.
- Eriksson, A.E., W.A. Baase, and B.W. Matthews. 1993. Similar hydrophobic replacements of Leu99 and Phe153 within the core of T4 lysozyme have different structural and thermodynamic consequences. *J. Mol. Biol.* 229:747–769.
- Flocco, M.M., and S.L. Mowbray. 1994. Planar stacking interactions of arginine and aromatic side-chains in proteins. *J. Mol. Biol.* 235:709–717.
- Gautam, M., and M.A. Tanouye. 1990. Alteration of potassium channel gating: molecular analysis of the *Drosophila Sh⁵* mutation. *Neuron*. 5:67–73.
- Hamill, O.P., A. Marty, E. Neher, B. Sakmann, and F.J. Sigworth. 1981. Improved patch-clamp techniques for high-resolution current recording from cells and cell-free membrane patches. *Pflügers Arch.* 391:85–100.
- Hodgkin, A.L., and A.F. Huxley. 1952. A quantitative description of membrane current and its application to conduction and excitation in nerve. *J. Physiol.* 117:500–544.
- Hoshi, T., W.N. Zagotta, and R.W. Aldrich. 1990. Biophysical and molecular mechanisms of *Shaker* potassium channel inactivation. *Science*. 250:533–538.
- Hoshi, T., W.N. Zagotta, and R.W. Aldrich. 1994. *Shaker* potassium channel gating I: transitions near the open state. *J. Gen. Physiol.* 103:249–278.
- Hurst, R.S., M.P. Kavanaugh, J. Yakel, J.P. Adelman, and R.A. North. 1992. Cooperative interactions among subunits of a voltage-dependent potassium channel. Evidence from expression of concatenated cDNAs. *J. Biol. Chem.* 267:23742–23745.
- Hurst, R.S., M.J. Roux, L. Toro, and E. Stefani. 1997. External barium influences the gating charge movement of *Shaker* potassium channels. *Biophys. J.* 72:77–84.
- Kamb, A., L.E. Iverson, and M.A. Tanouye. 1987. Molecular characterization of *Shaker*, a *Drosophila* gene that encodes a potassium channel. *Cell*. 50:405–413.
- Kanevsky, M. 1998. Role of the S5 Segment in Voltage Gating and Open State Stability of the *Shaker* Potassium Channel. Ph.D. Dissertation. Stanford University, Stanford, CA.
- Kavanaugh, M.P., R.S. Hurst, J. Yakel, M.D. Varnum, J.P. Adelman, and R.A. North. 1992. Multiple subunits of a voltage-dependent potassium channel contribute to the binding site for tetraethylammonium. *Neuron*. 8:493–497.
- Keynes, R.D., and F. Elinder. 1999. The screw-helical voltage gating of ion channels. *Proc. R. Soc. Lond. B Biol. Sci.* 266:843–852.
- Koren, G., E.R. Liman, D.E. Logothetis, G.B. Nadal, and P. Hess. 1990. Gating mechanism of a cloned potassium channel expressed in frog oocytes and mammalian cells. *Neuron*. 4:39–51.
- Larsson, H.P., O.S. Baker, D.S. Dhillon, and E.Y. Isacoff. 1996. Transmembrane movement of the *Shaker* K⁺ channel S4. *Neuron*. 16:387–397.
- Ledwell, J.L., and R.W. Aldrich. 1999. Mutations in the S4 region isolate the final cooperative step in *Shaker* potassium channel activation. *J. Gen. Physiol.* 113:389–414.
- Lichtinghagen, R., M. Stocker, R. Wittka, G. Boheim, W. Stühmer, A. Ferrus, and O. Pongs. 1990. Molecular basis of altered excitability in *Shaker* mutants of *Drosophila melanogaster*. *EMBO (Eur. Mol. Biol. Organ.) J.* 9:4399–4407.
- Liman, E.R., P. Hess, F. Weaver, and G. Koren. 1991. Voltage-sensing residues in the S4 region of a mammalian K⁺ channel. *Nature*. 353:752–756.
- Liman, E.R., J. Tytgat, and P. Hess. 1992. Subunit stoichiometry of a mammalian K⁺ channel determined by construction of multimeric cDNAs. *Neuron*. 9:861–871.
- Logothetis, D.E., B.F. Kammen, K. Lindpaintner, D. Bisbas, and G.B. Nadal. 1993. Gating charge differences between two voltage-gated K⁺ channels are due to the specific charge content of their respective S4 regions. *Neuron*. 10:1121–1129.
- Logothetis, D.E., S. Movahedi, C. Satler, K. Lindpaintner, and G.B. Nadal. 1992. Incremental reductions of positive charge within the S4 region of a voltage-gated K⁺ channel result in corresponding decreases in gating charge. *Neuron*. 8:531–540.
- Lopez, G.A., Y.N. Jan, and L.Y. Jan. 1991. Hydrophobic substitution mutations in the S4 sequence alter voltage-dependent gating in *Shaker* K⁺ channels. *Neuron*. 7:327–336.
- MacKinnon, R. 1991. Determination of the subunit stoichiometry of a voltage-activated potassium channel. *Nature*. 350:232–235.
- Mannuzzu, L.M., M.M. Moronne, and E.Y. Isacoff. 1996. Direct physical measure of conformational rearrangement underlying potassium channel gating. *Science*. 271:213–216.
- Marchais, D., and A. Marty. 1979. Interaction of permeant ions with channels activated by acetylcholine in *Aplysia* neurones. *J. Physiol.* 297:9–45.
- Matteson, D.R., and R.P.J. Swenson. 1986. External monovalent cations that impede the closing of K channels. *J. Gen. Physiol.* 87:795–816.
- McCormack, K., W.J. Joiner, and S.H. Heinemann. 1994. A characterization of the activating structural rearrangements in voltage-dependent *Shaker* K⁺ channels. *Neuron*. 12:301–315.
- McCormack, K., L. Lin, and F.J. Sigworth. 1993. Substitution of a hydrophobic residue alters the conformational stability of *Shaker* K⁺ channels during gating and assembly. *Biophys. J.* 65:1740–1748.
- McCormack, K., M.A. Tanouye, L.E. Iverson, J.W. Lin, M. Ramaswami, T. McCormack, J.T. Campanelli, M.K. Mathew, and B. Rudy. 1991. A role for hydrophobic residues in the voltage-dependent gating of *Shaker* K⁺ channels. *Proc. Natl. Acad. Sci. USA*. 88:2931–2935.
- Miller, C., R. Latorre, and I. Reisin. 1987. Coupling of voltage-dependent gating and Ba⁺⁺ block in the high-conductance, Ca⁺⁺-activated K⁺ channel. *J. Gen. Physiol.* 90:427–449.
- Moore, J.W., and S.H. Young. 1981. Dynamics of potassium ion currents in squid axon membrane. A re-examination. *Biophys. J.* 36:715–722.
- Neyton, J., and C. Miller. 1988. Discrete Ba²⁺ block as a probe of ion occupancy and pore structure in the high-conductance Ca²⁺-activated K⁺ channel. *J. Gen. Physiol.* 92:569–586.
- Neyton, J., and M. Pelleschi. 1991. Multi-ion occupancy alters gating in high-conductance, Ca⁽²⁺⁾-activated K⁺ channels. *J. Gen. Physiol.* 97:641–665.
- Noceti, F., P. Baldelli, X. Wei, N. Qin, L. Toro, L. Birnbaumer, and E. Stefani. 1996. Effective gating charges per channel in voltage-dependent K⁺ and Ca²⁺ channels. *J. Gen. Physiol.* 108:143–155.
- Papazian, D.M., T.L. Schwarz, B.L. Tempel, Y.N. Jan, and L.Y. Jan. 1987. Cloning of genomic and complementary DNA from *Shaker*, a putative potassium channel gene from *Drosophila*. *Science*. 237:749–753.
- Papazian, D.M., X.M. Shao, S.A. Seoh, A.F. Mock, Y. Huang, and D.H. Wainstock. 1995. Electrostatic interactions of S4 voltage sensor in *Shaker* K⁺ channel. *Neuron*. 14:1293–1301.
- Papazian, D.M., L.C. Timpe, Y.N. Jan, and L.Y. Jan. 1991. Alteration of voltage-dependence of *Shaker* potassium channel by mutations in the S4 sequence. *Nature*. 349:305–310.
- Perozo, E., R. MacKinnon, F. Bezanilla, and E. Stefani. 1993. Gating currents from a nonconducting mutant reveal open-closed conformations in *Shaker* K⁺ channels. *Neuron*. 11:353–358.

- Perozo, E., D.M. Papazian, E. Stefani, and F. Bezanilla. 1992. Gating currents in *Shaker* K⁺ channels. Implications for activation and inactivation models. *Biophys. J.* 62:160–168.
- Perozo, E., T.L. Santacruz, E. Stefani, F. Bezanilla, and D.M. Papazian. 1994. S4 mutations alter gating currents of *Shaker* K channels. *Biophys. J.* 66:345–354.
- Pongs, O., N. Kecskemethy, R. Muller, J.I. Krah, A. Baumann, H.H. Kiltz, I. Canal, S. Llamazares, and A. Ferrus. 1988. *Shaker* encodes a family of putative potassium channel proteins in the nervous system of *Drosophila*. *EMBO (Eur. Mol. Biol. Organ.) J.* 7:1087–1096.
- Rayner, M.D., J.G. Starkus, P.C. Ruben, and D.A. Alicata. 1992. Voltage-sensitive and solvent-sensitive processes in ion channel gating. Kinetic effects of hyperosmolar media on activation and deactivation of sodium channels. *Biophys. J.* 61:96–108.
- Sala, S., and D.R. Matteson. 1991. Voltage-dependent slowing of K channel closing kinetics by Rb⁺. *J. Gen. Physiol.* 98:535–554.
- Salkoff, L. 1983. Genetic and voltage-clamp analysis of a *Drosophila* potassium channel. *Cold Spring Harbor Symp. Quant. Biol.* 1:221–231.
- Sanger, F., S. Nicklen, and A.R. Coulson. 1977. DNA sequencing with chain-terminating inhibitors. *Proc. Natl. Acad. Sci. USA.* 74:5463–5467.
- Schauf, C.L., and J.O. Bullock. 1979. Modifications of sodium channel gating in *Myxicola* giant axons by deuterium oxide, temperature, and internal cations. *Biophys. J.* 27:193–208.
- Schauf, C.L., and J.O. Bullock. 1980. Solvent substitution as a probe of channel gating in *Myxicola*. Differential effects of D₂O on some components of membrane conductance. *Biophys. J.* 30:295–305.
- Schoppa, N.E., K. McCormack, M.A. Tanouye, and F.J. Sigworth. 1992. The size of gating charge in wild-type and mutant *Shaker* potassium channels. *Science.* 255:1712–1715.
- Schoppa, N.E., and F.J. Sigworth 1998a. Activation of *Shaker* potassium channels. I. Characterization of voltage-dependent transitions. *J. Gen. Physiol.* 111:271–294.
- Schoppa, N.E., and F.J. Sigworth. 1998b. Activation of *Shaker* potassium channels. II. Kinetics of the V2 mutant channel. *J. Gen. Physiol.* 111:295–311.
- Schoppa, N.E., and F.J. Sigworth 1998c. Activation of *Shaker* potassium channels. III. An activation gating model for wild-type and V2 mutant channels. *J. Gen. Physiol.* 111:313–342.
- Schulz, G.E., and R.H. Schirmer. 1979. Principles of Protein Structure. Springer-Verlag, New York. 314 pp.
- Seoh, S.A., D. Sigg, D.M. Papazian, and F. Bezanilla. 1996. Voltage-sensing residues in the S2 and S4 segments of the *Shaker* K⁺ channel. *Neuron.* 16:1159–1167.
- Shao, X.M., and D.M. Papazian. 1993. S4 mutations alter the single-channel gating kinetics of *Shaker* K⁺ channels. *Neuron.* 11:343–352.
- Shieh, C.C., K.G. Klemic, and G.E. Kirsch. 1997. Role of transmembrane segment S5 on gating of voltage-dependent K⁺ channels. *J. Gen. Physiol.* 109:767–778.
- Sigg, D., and F. Bezanilla. 1997. Total charge movement per channel. The relation between gating charge displacement and the voltage sensitivity of activation. *J. Gen. Physiol.* 109:27–39.
- Sigg, D., E. Stefani, and F. Bezanilla. 1994. Gating current noise produced by elementary transitions in *Shaker* potassium channels. *Science.* 264:578–582.
- Sigworth, F.J. 1994. Voltage gating of ion channels. *Q. Rev. Biophys.* 27:1–40.
- Smith-Maxwell, C.J., J.L. Ledwell, and R.W. Aldrich. 1998a. Role of the S4 in cooperativity of voltage-dependent potassium channel activation. *J. Gen. Physiol.* 111:399–420.
- Smith-Maxwell, C.J., J.L. Ledwell, and R.W. Aldrich. 1998b. Uncharged S4 residues and cooperativity in voltage-dependent potassium channel activation. *J. Gen. Physiol.* 111:421–439.
- Spruce, A.E., N.B. Standen, and P.R. Stanfield. 1989. Rubidium ions and the gating of delayed rectifier potassium channels of frog skeletal muscle. *J. Physiol.* 411:597–610.
- Starkus, J.G., T. Schlieff, M.D. Rayner, and S.H. Heinemann. 1995. Unilateral exposure of *Shaker* B potassium channels to hyperosmolar solutions. *Biophys. J.* 69:860–872.
- Stefani, E., L. Toro, E. Perozo, and F. Bezanilla. 1994. Gating of *Shaker* K⁺ channels: I. Ionic and gating currents. *Biophys. J.* 66:996–1010.
- Swenson, R.P.J., and C.M. Armstrong. 1981. K⁺ channels close more slowly in the presence of external K⁺ and Rb⁺. *Nature.* 291:427–429.
- Tagliatela, M., L. Toro, and E. Stefani. 1992. Novel voltage clamp to record small, fast currents from ion channels expressed in *Xenopus* oocytes. *Biophys. J.* 61:78–82.
- Tanouye, M.A., and A. Ferrus. 1985. Action potentials in normal and *Shaker* mutant *Drosophila*. *J. Neurogenet.* 2:253–271.
- Tanouye, M.A., A. Ferrus, and S.C. Fujita. 1981. Abnormal action potentials associated with the *Shaker* complex locus of *Drosophila*. *Proc. Natl. Acad. Sci. USA.* 78:6548–6552.
- Tempel, B.L., D.M. Papazian, T.L. Schwarz, Y.N. Jan, and L.Y. Jan. 1987. Sequence of a probable potassium channel component encoded at *Shaker* locus of *Drosophila*. *Science.* 237:770–775.
- Tytgat, J., and P. Hess. 1992. Evidence for cooperative interactions in potassium channel gating. *Nature.* 359:420–423.
- Wu, C.F., and F.N. Haugland. 1985. Voltage clamp analysis of membrane currents in larval muscle fibers of *Drosophila*: alteration of potassium currents in *Shaker* mutants. *J. Neurosci.* 5:2626–2640.
- Xu, J., W. Yu, J.M. Wright, R.W. Raab, and M. Li. 1998. Distinct functional stoichiometry of potassium channel beta subunits. *Proc. Natl. Acad. Sci. USA.* 95:1846–1851.
- Yang, N., A.J. George, and R. Horn. 1996. Molecular basis of charge movement in voltage-gated sodium channels. *Neuron.* 16:113–122.
- Yang, N., and R. Horn. 1995. Evidence for voltage-dependent S4 movement in sodium channels. *Neuron.* 15:213–218.
- Yang, Y., Y. Yan, and F.J. Sigworth. 1997. How does the W434F mutation block current in *Shaker* potassium channels? *J. Gen. Physiol.* 109:779–789.
- Yusaf, S.P., D. Wray, and A. Sivaprasadarao. 1996. Measurement of the movement of the S4 segment during the activation of a voltage-gated potassium channel. *Pflügers Arch.* 433:91–97.
- Zagotta, W.N., and R.W. Aldrich. 1990a. Voltage-dependent gating of *Shaker* A-type potassium channels in *Drosophila* muscle. *J. Gen. Physiol.* 95:29–60.
- Zagotta, W.N., and R.W. Aldrich. 1990b. Alterations in activation gating of single *Shaker* A-type potassium channels by the *Shr^s* mutation. *J. Neurosci.* 10:1799–1810.
- Zagotta, W.N., T. Hoshi, and R.W. Aldrich. 1994b. *Shaker* potassium channel gating. III: Evaluation of kinetic models for activation. *J. Gen. Physiol.* 103:321–362.
- Zagotta, W.N., T. Hoshi, J. Dittman, and R.W. Aldrich. 1994a. *Shaker* potassium channel gating. II: Transitions in the activation pathway. *J. Gen. Physiol.* 103:279–319.
- Zimmerberg, J., F. Bezanilla, and V.A. Parsegian. 1990. Solute inaccessible aqueous volume changes during opening of the potassium channel of the squid giant axon. *Biophys. J.* 57:1049–1064.
- Zimmerberg, J., and V.A. Parsegian. 1986. Polymer inaccessible volume changes during opening and closing of a voltage-dependent ionic channel. *Nature.* 323:36–39.
- Zimmerberg, J., and V.A. Parsegian. 1987. Water movement during channel opening and closing. *J. Bioenerg. Biomembr.* 19:351–358.